Modelling mastication and aroma release from white rice during food oral processing

Syahmeer How, Jim R Jones, Marco P Morgenstern, Eli Gray-Stuart, John Bronlund, Anne Saint-Eve, Ioan-Cristian Trelea, Isabelle Souchon

Modelling mastication and aroma release from white rice during FOP

*Syahmeer How[1], Jim R. Jones[2], Marco P. Morgenstern[3,4], Eli Gray-Stuart[2], John E. Bronlund[2,3], Anne Saint-Eve[5], Ioan Cristian Trelea[5], Isabelle Souchon[6]

1. Department of Process and Food Engineering, Faculty of Engineering, Universiti Putra Malaysia, Selangor Darul Ehsan, Malaysia
2. Department of Chemical and Bioprocess Engineering, School of Food and Advanced Technology, Massey University, Palmerston North, New Zealand
3. Riddet Institute, Palmerston North, New Zealand
4. New Zealand Institute for Plant and Food Research, Lincoln, New Zealand
5. Université Paris-Saclay, INRAE, AgroParisTech, UMR SayFood, F-78850, Thiverval-Grignon, France
6. UMR408 SQPOV, INRAE, Avignon Université, F-84000 Avignon, France

***Corresponding author email address** : syahmeerhow@upm.edu.my*

Abstract

A mathematical model describing the aroma release from white rice during food oral processing (FOP) was developed based of a coupled selection-breakage and mass transport models. An integrated selection and breakage model was able to predict the changes of bolus surface area over time, assuming that the pasted portion of masticated rice particles was the dominant mechanism when aroma was released to the liquid bolus during chewing. Model predictions were validated against experimental data for all subjects when the input parameters were directly obtained from the coupled chewing-aroma release model. Adjusting the input parameters from one of the validated coupled model showed that the portion size,

initial concentration of the studied aroma compound, initial liquid volume and the rice pasted fraction were the most sensitive product-related parameters. The oral cavity volume, pharynx volume, nasal cavity volume and the breathing frequency were the most sensitive physiological parameters. The physico-chemical parameter which had the most significant effect was the mass transfer coefficient in the saliva phase.

Keywords;

Particle Size Distribution; Paste; Bolus surface area; Mass transfer; Mastication; Ordinary Differential Equations

1. Introduction

Mathematical models have been developed in the literature to predict the aroma release of various food matrix types during FOP. Harrison et al. (1998) provided the first model for predicting the aroma release of solid and semisolid foods. However, the model lacked experimental validation. Strong simplifying assumptions were made for the suggested model such as constant breath airflow and the model application was limited to the type of solid and semi-solid foods that retained their shape and did not further disintegrate into the surrounding saliva with increasing chewing cycles (Harrison et al., 1998; Trelea et al., 2007). Since Harrison et al. (1998), improvements have been made by incorporating a more realistic description of physiological mechanism, such as for mastication of semi-solid products (Wright & Hills, 2003; Wright et al., 2003; Trelea et al., 2007; Doyennette et al., 2014; Harrison et al., 2014) and for liquid products (Rabe et al., 2004; Doyennette et al., 2011; Le Révérend et al., 2013).

The most comprehensive model to predict aroma release during oral processing of semi-solid foods to date was developed by Doyennette et al. (2014). The model was constructed using one-dimensional differential equations for mass transfer and flavour release and was validated against experimental *in vivo* data using cheese as the food system. A sensitivity analysis performed on the mathematical model showed that the air-bolus contact surface area could affect aroma release; however, the model did not include the coupling to any food breakdown model to predict the air-bolus contact surface area. Due to fragmentation caused by mastication, where food particles are reduced in size, the model assumes that the contact area between the solid product and the liquid bolus during mastication evolves linearly with time. The authors acknowledged that this was a simplified assumption, as the exact rate of change of contact area is not known for products such as cheese and rice, where when ingested, a fraction of the food product can form very fine particles that can dissolve in

the liquid phase of the bolus due to the combined action of mastication, saliva incorporation and the warming of the product in the mouth, known as the pasted fraction (Doyennette et al., 2014; How et al., 2021). The limitation of the model was acknowledged by the authors as the lack of coupling to a dynamic food breakdown model to predict the particle size distribution with respect to chew number stating that validating the model would require complex experimental protocols which are challenging to execute (e.g. bolus spitting after a variable number of bites).

The aim of the study was to develop a model that could accurately describe how the concentration of aroma release changes over time during mastication of cooked white rice. The work carried out here is limited to predicting the volatile components of released aroma in the nasal cavity, rather than those related to taste, which is a subject of ongoing work. This work is an extension to our previous study investigating the role of oral processing on *in vivo* aroma release of rice by comparing experimental results with a conceptual model (How et al., 2021). The main novelty of the model developed in this study compared to previous aroma release models developed in the literature is the coupling of a food breakdown model based of an integrated mechanistic selection and breakage functions (How et al., 2022) to predict the air-bolus contact area in the mouth compartment. Selection is the probability per chew that food particles are damaged or broken and has been shown to depend on particle size and number through the one-way and two-way competition models (van der Glas et al., 1992, 2018). Breakage is the distribution function of the daughter particles that originate from each selected particle which could be described using mechanistic and empirical functions (Austin, 1971; van der Bilt el al., 1987; van der Glas et al., 1987; Gray-Stuart, 2016). To ensure conservation of volume after breakage of particles, a discretised population balance method is commonly employed to track selection and breakage of individual particles (Gray-Stuart, 2016; How et al., 2022).

In addition to the food breakdown aspect, the model would have to consider the mechanisms for mass transfer between the solid particles and liquid content of the bolus and how the interfacial area between the bolus and air phases change during mastication. In this study, the model was validated by comparing the model simulations to *in vivo* aroma release data of cooked white rice flavoured with two food grade aroma compounds (2-nonanone and ethyl propanoate), measured by Proton Transfer Reaction-Mass Spectrometry (PTR-MS) in real time on five panellists.

2. Conceptual model development

Figure 1 shows the conceptual diagram for the interconnected compartments that are involved in aroma release during the consumption of cooked white rice. Refer to Appendix A1 for the nomenclature table. The compartments that were involved in flavour release during food consumption were denoted as follows: the oral cavity (index O), the pharynx (index F), the nasal cavity (index N) and the trachea (index T). The model used here is an adaptation from a chemical engineering approach where the various parts of the upper respiratory tract are viewed as interconnected reactors, containing an air phase (index A) and the saliva phase, index (S). To take the retention effect of lubricated mucosa (index M) into account, the lubricated mucosa layers were also included in each compartment (oral cavity, pharynx and nasal cavity). The compartments were included as one of the aroma compounds used to spike the cooked white rice, 2-nonanone, was known to interact with the lubricated mucosa (Doyennette et al., 2014; Déléris et al., 2016). The airflow rates (Q_{Na}, Q_{Ta}, Q_{Oa}), were considered to be positive if their direction is the one indicated by the arrows in Figure 1 (inhalation) and negative when in the opposite case (exhalation).

Aroma concentrations in all compartments (oral cavity, pharynx and nasal cavity) were calculated using mass transfer equations and mass balances. The mass balances include the

flavour release at the saliva – product (rice) interface, air-saliva interface and the air and lubricated mucosa layer interface. In general, when two phases are in contact (e.g. air and saliva), volatile transfer occurs across the interfacial layers. At each side of the interface, the driving force is the concentration difference between the bulk phase and the interface. At the infinitely thin interface, local equilibrium is expressed via the partition coefficient between phases. The released volatile flux will depend on the contact area between phases and the transfer resistance in each phase, expressed via mass transfer coefficients. Other than the interfacial release, bulk flow may also occur between the various compartments. The volatile mass balances for this case involve the bulk concentrations and the bulk flow rates.

2.1 Assumption of the contact area between the rice and saliva phase

We assumed that the breakdown of a cooked rice particle during mastication follows a 'cleave and paste' mechanism. In this mechanism, rice kernel when occluded between opposing molars are assumed to produce one or a several large particles, and a fraction of the original kernel is pasted into very fine particles (paste) which become effectively part of the liquid phase of the bolus. As described in our previous work in How et al. (2021), it was found that during the mastication of rice, the bolus forms a bimodal particle size distribution (PSD) when measured using a laser diffraction method. It follows that particles with a size less than 0.355 mm were not broken down in subsequent chewing cycles (i.e. pastes), which are assumed to be individual separated swollen starch granules. Pasting involves swelling of granules and it is known that native rice starches have granule sizes in the range of 1.9–26 μm. During cooking, the granule can swell 2 to 48 times of their initial size when heated to various temperatures (How et al. 2021). Therefore the threshold of 0.355 mm used as an assumption when particles become pastes simplifies the model.

Therefore, during mastication of rice, two simultaneous phenomena can occur:

- the transfer of aroma compounds from the non-pasted daughter particles into the liquid phase of the bolus, particularly from newly exposed surface area generated during a chewing cycle, and
- the release of the aroma compounds contained in the pasted particles into the liquid phase of the bolus, where it was assumed because of the small size, that once transferred, the concentration of the aroma compounds in the pasted and liquid phases reach equilibrium instantaneously.

The direct transfer of aroma compounds from the solid surfaces into the air phase was assumed negligible as after ingestion there will be at least a thin layer of saliva/moisture present between these two phases and therefore aroma transfer always takes place through the liquid phase.

Because of the challenge to distinguish between the relative contributions of each mechanism, it was assumed that the release of the aroma compounds was dominated by the transfer of the aroma compounds from the pasted particles into the liquid phase of the bolus. This was a reasonable assumption as the surface area to volume ratio of the pasted particles will be significantly larger than the surface area to volume ratio of the particles that were greater than 0.355 mm. Similarly the distances for diffusion in the pasted particles was very small. Thus, it is expected that the transfer of the aroma compounds from the pasted particles to the liquid phase of the bolus is significantly faster compared to the transfer from the larger particles.

Once in the liquid phase of the bolus, the concentration of the aroma compounds will be diluted by saliva flow into the oral cavity (Harrison et al., 1998). At the same time, volatiles partition from the saliva into the air phase which then transports them to the pharyngeal compartment. During mastication, some aroma release to the pharynx and further to the nasal cavity is possible for panellists with imperfect velopharyngeal closure (Trelea et al., 2007). In

the model, it is assumed that all subjects possess an imperfect velopharyngeal closure if the concentration of aroma compounds increases after food ingestion and continues to do so during the mastication period (i.e. the period before swallowing).

2.2 Other model assumptions

Further to the assumptions described above, the following additional assumptions were made to develop the model equations.

- The assumptions for the aroma release model from oral, pharyngeal and nasal cavities during consumption of solid (chewed) products were described in detail in Doyennette et al., 2014.
- The assumptions for the integrated selection and breakage model to predict PSD of rice particles during FOP have been described in detail in How et al., 2022.
- The assumptions concerning the interaction of the two models were as follows:
    - Food oral processing took place in isothermal conditions. That is, the temperature of the cooked rice which was served at 37^{o}C, was constant throughout the duration of mastication. This is a reasonable assumption, considering the body temperature is at 37^{o}C. This assumption also ensures the partition coefficient of aroma compounds will not change with temperature and avoids the need to include a heat transfer model.
    - Food particles in the mouth were immediately coated with saliva at time zero and after each chew when new surface area of particles were generated by food breakage.
    - It was assumed that due to a relatively short mastication time, α-amylase had zero or minimal contribution to the mass transfer coefficient of aroma compounds by decreasing the bolus viscosity.

- The properties of the aroma compounds, such as the partition coefficient, were not affected by the variations in saliva compositions between individuals and by interaction with food components.

3. Formulation of model equations

The aroma release model equations used in this study are based on the one described in detail in Doyennette et al. 2014 and the integrated selection and breakage models are based on How et al. 2022. The main equations related to the interaction of the two models are given below and the full set of equations are reported in appendices A2 and A3 respectively.

3.1 Liquid bolus in the oral cavity

The liquid bolus compartment is initially composed of pure saliva and is progressively flavoured by the addition of rice particles which were pasted. The volume increases by the addition of saliva (salivary flow rate) and with the addition of pasted particles.

The volume of the liquid bolus $V_{Ol(t)}$ can then be divided into two parts:

$$V_{Ol(t)} = V_{Os(t)} + V_{Opasted(t)} \#(1)$$

where

$$\frac{dV_{Os(t)}}{dt} = Q_{Os} \#(2)$$

3.2 Concentration of aroma compounds in the saliva phase

After each chewing cycle, a new volume of pasted particles are formed. These were then added to saliva, which form the liquid bolus. The concentration of the aroma compounds in the saliva phase and pasted particles were assumed to reach equilibrium instantaneously. Therefore, after each chewing cycle, the mass of the aroma compounds in the saliva phase is

a combination of the initial mass (before chewing) and the new mass of aroma being added from the pasted particles. Hence,

$$V_{Os_i}C_{Os_i} + V_{Opasted_i}C_{Opasted_i} + \left(V_{Opasted_{i+1}} - V_{Opasted_i}\right)C_{op} = V_{Os_{i+1}}C_{Os_{i+1}} + V_{Opasted_{i+1}}C_{Opasted_{i+1}} \# \quad \ldots(3)$$

The volatile concentration on the pasted particles side, using the partition conditions at the interface, is given by

$$C_{Opasted} = \frac{C_{Os}}{K_{Osp}} \#(4)$$

After rearranging, the concentration of the aroma compound in the saliva after a single chew can be described as

$$C_{Os_{i+1}} = \frac{(V_{Os} + \frac{V_{Opasted}}{K_{Osp}})_i C_{Os_i} + \left(V_{Opasted_{i+1}} - V_{Opasted_i}\right)C_{Op}}{(V_{Os} + \frac{V_{Opasted}}{K_{Osp}})_{i+1}} \#(5)$$

This step change in aroma concentration occurs instantaneously with each chew and then changes dynamically due to dilution with the addition of saliva or losses to the oral airspace. Thus,

$$\frac{dC_{Os}(t)}{dt} = \frac{-\left(Q_{Os}C_{Os}(t) + A_{Ob}(t)k_{Os}\left(C_{Os}(t) - \frac{C_{Oa}(t)}{K_{Oas}}\right)\right)}{\left(V_{Os}(t) + \frac{V_{Opasted}(t)}{K_{Osp}}\right)} \#(6)$$

3.3 Bolus surface area

For clarity to the reader, only the main equations used to predict the bolus surface area are described in this section. Full explanation is given in Appendix A3.

The bolus surface area was predicted by adapting the concept of a sintering mechanism which is used in forming metal, ceramic, polymer and composite components from particles (German, 2016). In a sintering mechanism, the total surface area of the particles is reduced by growing bonds (bridges) between contacting particles during a heating process. The same concept was applied to model the bolus surface area. As the number of chews increases, the amount of saliva incorporated in the bolus also increases. This also increases the number of saliva bridges among the particles in the bolus, which promotes the merge of particles. For the sintering mechanism, a linear relationship was proposed between the surface area and the packing density where the surface area declines as the density increases (German, 2016). Thus, the surface area of a bolus can be described as

$$A_{Ob} = \frac{SA_{sphere} - SA_E}{1 - \emptyset_E}(\emptyset - 1) + SA_{sphere} \#(7)$$

where SA_E is the initial surface area of the bolus, which is the summation of all surface area of individual rice particles predicted using the integrated selection and breakage functions (How et al., 2022). As individual particles merge with the help of liquid saliva bridges to form a bolus, the total surface area of the bolus decreases. The bolus saturation, S decides when Eq. 7 is used to estimate the bolus surface area where

$$S = \frac{V_{opasted} + V_s}{V_{ptotal}} . \left(\frac{1 - \varepsilon}{\varepsilon}\right) \#(8)$$

For any saturation value less than 1, Eq. 8 will be used to estimate the bolus surface area. For the bolus when the saturation surpasses the value of 1, the bolus surface area was estimated by assuming the bolus is of a spherical shape where

$$SA_{sphere} = 4\,\pi\, R^{\frac{2}{3}} \#(9)$$

3.3.1 Selection and Breakage model

The chewing model used to predict A_{Ob} in Eq. 7 consists of selection and breakage sub-models. The mechanistic one-way and two-way competition selection models (van der Glas et al., 1992, 2018; How et al., 2022) were initially applied and compared to identify which model that best fits the experimental data. The breakage function used in the chewing model was as described in Eq. 10 below which was previously applied on brown rice (Gray-Stuart, 2016). The equation assumes that the pasted fraction is constant.

$$B(X, X_0) = (1 - P).\left[1 - \left(1 + r.\frac{X}{X_0}\right).\left(1 - \frac{X}{X_0}\right)^r\right] \#(10)$$

The PSD was predicted using the discretised population balance model and is described in detail in How et al. (2022).

3.4 Initial conditions

The initial concentration of aroma compounds in all compartments for the when the product was introduced in the mouth up to the first chewing cycle (chew 0 to chew 1), is zero. The initial volume of saliva to solve Eq. 2 was set as the volume of saliva at rest. Thus, the initial conditions from chew 0 to chew 1 are:

$$V_{Os}(t_0) = V_{Osrest}$$

$$C_{Os}(t_0) = C_{Oa}(t_0) = C_{Om}(t_0) = C_{Fs}(t_0) = C_{Fm}(t_0) = C_{Fa}(t_0) = C_{Nm}(t_0) = C_{Na}(t_0) = 0$$

After the 1st chew, rice will break into smaller particles, and some will be pasted which dissolves in the liquid bolus. The volatiles from the pasted particles are then transferred into the liquid bolus, and an instant equilibrium was assumed (see section 2.1).

Thus, the initial conditions of the model following the first chew are:

253 $$C_{Os}(t_0) = C_{Os}(t_{chew=1})$$ calculated from Eq. 5

$$V_{Os}(t_0) = V_{Os}(t_{chew=1})$$

$$C_{Oa}(t_0) = C_{Oa}(t_{chew=1})$$

$$C_{Om}(t_0) = C_{Om}(t_{chew=1})$$

$$C_{Fs}(t_0) = C_{Fs}(t_{chew=1})$$

$$C_{Fm}(t_0) = C_{Fm}(t_{chew=1})$$

$$C_{Fa}(t_0) = C_{Fa}(t_{chew=1})$$

$$C_{Nm}(t_0) = C_{Nm}(t_{chew=1})$$

$$C_{Na}(t_0) = C_{Na}(t_{chew=1})$$

254

255 ### *3.5 Model numerical solution*

256 The model was solved numerically using MATLAB program version R2019a using ode45
257 solver with a default relative error tolerance value of 0.001 which was shown to produce
258 negligible numerical error.

259 # 4. Experimental methods

260 ### *4.1 Food system*

261 White Jasmine rice (Oryza sativa L.) was used as the test food system of the model. Cooked
262 rice is aromatic and forms a particulate bolus with high bolus recovery (80-95%) which
263 allows the coupled selection-breakage and aroma models to be used (How et al., 2021). The
264 cooking method followed the procedure described in How et al. 2021 where it was cooked
265 using a 1:2 ratio, cooked in a microwave rice steamer. The rice was also cooked in three
266 batches to check the repeatability of the cooking method, where the moisture content (61

g/100 g of sample, average of three samples) showed ± 0.9% variation between batches. Approximately 5 g of cooked rice samples were transferred into small containers and were kept warm at 60 °C. The rice was served to the subjects after cooling down to approximately 50 °C, which is the temperature at which rice is usually consumed (How et al., 2021).

4.2 Subject's physiological characteristics

The physiological characteristics are critical input parameters required to predict aroma release. The input parameters were determined from the experimental measurements made in How et al. (2021) or from the information found in the literature. Appendix A6 summarises the physiological parameters required for the model, the values used and their source.

The oral cavity volume, V_{Oamean}, the volume of air in the pharynx, V_{Fa} and the volume of air in the nasal cavity,V_{Na} were measured using the rhinopharyngometer as described in Doyennette et al. (2014). The volume of saliva at rest, V_{Osrest} and the saliva flow rate, Q_{Os} were obtained from the y-intercept and the slope of the subject's bolus saliva content and chew number relationship based on the method previously discussed in detail in Motoi et al. (2013). The number of chews required to reach swallow point, $n_{chews,}$ the chewing frequency, fr_{chew} and the time taken to swallow, $t_{swallow}$ for each subject during the *in vivo* aroma release experiment were determined according to the protocol as previously described in How et al. (2021).

The breathing frequency of the panellists during the consumption of the cooked rice was estimated from the acetone signal (*m/z 59*) measured in the nasal cavity which was recorded synchronously with the concentration of the target aroma compounds (Trelea et al., 2007). The breathing frequency was determined by measuring the time it takes to complete one breathing cycle. This was determined by identifying the point when the signal decreases and increases, as it symbolises when the subject inhales and exhales. The breathing frequency

used in the model was the average of five replicates of breathing frequencies. Other physiological variables including the area of the mucosa in all compartments (oral cavity, pharynx and nasal cavity), the thickness of the mucosa layer, and the breath volume/tidal volume were determined from the literature.

4.3 Physico-chemical model input parameters

Other input parameters required for the model include the physico-chemical properties of the aroma compound that was flavoured in the cooked rice, such as the partition coefficient between different phases. The air/rice partition coefficient at 37 ^{o}C and the initial concentration of the studied aroma compounds were determined using the phase ratio variation (PRV) method by headspace chromatography (Atlan et al., 2006; Doyennette et al., 2011). Further explanation are given in Mohd Firdaus How (2021), Chapter 9. The mass transfer coefficient was also required to predict aroma release, which was obtained from the literature. Appendix A7 summarises the remaining parameters required for the model.

4.4 Chewing model input parameters

The initial PSD of 5 grams of rice (How et al., 2021) was used as the starting distribution in the model. The size of particles were between 5-6.5 mm of diameter (Mohd Firdaus How, 2021). The input parameters required for the one-way and two-way selection functions are the number of particles, the number of breakage sites and the affinity factor. When considering the possibility of particle piling between antagonistic posterior teeth during jaw-closing for the two-way interaction model, particle height, i.e. thickness or intermediate diameter is relevant because the length axis of the rice grains will approximately parallel to the occlusal plane between antagonistic teeth. It was found in van der Bilt et al. (1991) and van der Glas et al. (2018) that particles can only pile when their height are smaller than 4 mm. In this study, assuming that the rice grains followed a similar aspect ratio of 3.3 ± 0.3 as reported in Yu et al. (2019), the thickness (smallest diameter) or intermediate diameter of the

316 grains will be about 1.7 mm. Therefore, the piling conditions are completely favourable for
317 the two-way interaction model due to a small initial particle height of about 1.7 mm of rice
318 grains. As such, for efficiency, the two-way interaction model was used to describe the
319 selection process in the integrated selection-breakage model.

320 The degree of fragmentation variable and the pasted fraction are required for the breakage
321 function (section 3.3.1).

322 ### 4.4.1 Selection-Breakage model fitting using Particle Swarm Optimisation
323 (PSO)

324 Using the initial PSD as described above as the input to the model, the rice bolus PSD after 1
325 chew, 2 chew, 25%, 50%, 75% and 100% of swallow point was determined for each subject.
326 The PSD of the bolus samples was analysed by image analysis following the procedure
327 described in How et al. (2021), which provided the projected area of individual particles in
328 mm^2. To transform the projected area (2D) to volume (3D), it was assumed that each rice
329 particle was of cylindrical shape, where the volume was determined by multiplying the
330 projected area with an assumed height. The height was obtained by multiplying the
331 characteristic dimension of the projected area with a factor. A circular shape was assumed to
332 determine the characteristic dimension of the projected area (diameter in mm). Thus,

$$V = h.A \#(11)$$

333

334 where V is the volume of a particle in mm^3, h is the assumed height in mm, and A is the
335 projected area of a particle in mm^2. The constant h is determined by the following equation

$$h = f.\left(\frac{4.A}{\pi}\right)^{\frac{1}{2}} \#(12)$$

336

337 where f is a factor. The factor f was obtained by minimising the residual sum of squares
338 between the total predicted volume of particles calculated using equation 11 and the

experimental recovered volume of bolus (Gray-Stuart, 2016; Zheng et al., 2021). While the assumption of a cylindrical shape rice particles provided a simple starting point in this study, a more realistic shape for rice such as ellipsoidal (Yu et al., 2019) could be used in the future where the ratios between the major and minor axes could also be assessed on the basis of experimental data.

Due to the large number of model parameters to be solved, PSO algorithm was deployed to solve the model input parameters by minimising the normalised sum of squares residuals between the model and the experimental data. PSO has been used in food-related optimisations such as modelling spray drying of coconut milk, mastication of peanuts and more recently in the optimisation of restaurant atmosphere by coupling with Artificial Neural Network (Ming et al., 2021; How et al., 2022; Kantono, How & Wang., 2022). The residual was calculated from 10 d-values that were the intercepts for 10% (d10), 20% (d20) 30% (d30), 40% (d40), 50% (d50), 60% (d60), 70% (d70), 80% (d80), 90% (d90) of the cumulative volume distribution of the model and the experimental data. The algorithm was also solved to minimise the normalised residual of the pasted fraction (defined as the volume fraction for particles less than 0.354 mm) of the model and experimental data. Due to the probabilistic nature of the way the selection and breakage models were implemented, the model was repeated for 50 times and the average was determined to calculate the residual for the model fitting (How et al., 2022).

4.5 *In vivo* aroma release data for model validation

Aroma release of five panellists' were measured using PTR-MS (Ionicon Analytik, Innsbruck, Austria). These was the same data collected in our previous study in How et al. (2021) where a minimum of five replicates were performed for all *in vivo* measurements. In previous studies involving the modelling of aroma release, the model prediction is compared against experimental measurements by representing the data as a peak line (Doyennette et al.,

2011; Doyennette et al., 2014). This is done by smoothing the breath-by-breath aroma release profiles by plotting a curve linking the maxima of the sinusoids (Doyennette et al., 2011). However, due to a longer sampling time nature of the experimental data and lack in consistency to when sampling was initiated relative to breathing (further explanation in Chapter 9 of Mohd Firdaus How. (2021)), the cumulative area under the curves of both model simulations and experimental data (normalised concentrations by dividing concentration against maximum concentration) were compared for validation.

5. Results and Discussions

5.1 Selection-Breakage model fitting

Table 1 below shows the comparison of the best-fit input parameter results when the breakage function of Eq. 10 and when the two-way competition selection model were applied (How et al., 2022). The R-squared was calculated as described in How et al. 2022. Figure 2 shows the model fits for Subject A4. For clarity to readers, comparisons between the fitted *d*-values and pasted fraction against experimental data for all of the five subjects are shown in Appendix A4.

For most of the subjects, a better fit was achieved when the two-way competition model was used as the selection model. This is supported by the higher R-squared values when the two-way competition model was used across most subjects in Table 1. Subject A1 however had a better fit when the one-way competition model was used as it had a greater number of larger particles (particles between 4-5.7 mm) compared to other subjects even at the later stages of mastication (Appendix A4).

5.2 Validation of the coupled selection breakage-mass transport models

.The PSD outputs from the selection-breakage model were then used to calculate the volume of the pasted particles and the total surface area of particles as they were the variables

388 required to couple with the mass transport models.. Similarly, the physiological input
389 parameters of each subjects and the physicochemical parameters as described in the
390 experimental methods were applied. The cumulative area under the curve were then obtained
391 for the normalised concentrations of 2-nonanone (*m/z 143*) and ethyl propanoate (*m/z 103*) in
392 the nasal cavity.

393 The main assumption of the model is that during chewing, aroma compounds are transferred
394 to the saliva phase from the pasted rice particles instantaneously. The size threshold for when
395 rice particles are pasted was set as 0.354 mm by Gray-Stuart (2016) in his work. Here, the
396 model was predicted using different pasted size thresholds (0.2 mm, 0.354 mm, 0.5 mm and
397 when all particles are pasted) and compared against the experimental data to see if the
398 difference in the threshold has a pronounced effect on the prediction. The five replicates of
399 the experimental data were compared against the model prediction. It should be considered
400 that for the particle breakdown model the threshold was set to describe particles that become
401 too small to be actively broken down by occlusion. In terms of aroma release, the pasted
402 particle threshold corresponds to particles that are assumed to instantaneously equilibrate
403 their aroma compound with the liquid portion of the bolus. Figure 3 shows the comparison of
404 the model predictions against the experimental data for one of the subjects tested in the study
405 (subject A4). The results for the rest of the subjects are shown in Appendix A5. A common
406 trend can be seen from all figures is that the model predictions satisfactorily agreed with the
407 experimental data well for ethyl propanoate (*m/z 103*) compared to 2-nonanone (*m/z 143*).
408 When compared against different size thresholds,

409 ### *5.3 Using the integrated selection-breakage and mass transport models to*
410 ### *provide insights for food design*
411

412 Figure 4 shows the effects of some parameters related to the product and to the individual to
413 the aroma release (concentration of aroma compound in the nasal cavity, C_{na}) which could be

414 of interest to a food manufacturer. For clarity to readers, the results for subject A4 are used
415 here as a reference.

416 It can be observed when the portion size increased (Figure 4 a), C_{na} increased. This is
417 expected as the higher the portion size, the higher the volume of particles which will be
418 broken into pasted particles during mastication. This is consistent with the main model
419 assumption which assumes mass transfer of aroma compounds had only occurred from the
420 paste to the saliva phase. Therefore, the higher the volume of particles that are pasted, the
421 higher the C_{na}. The same trend can be observed when the initial particle size is varied (Figure
422 4 b). The larger the particle size, the higher the volume of a particle. Thus, the higher the
423 volume of pasted particles will be formed, which result to a higher C_{na}. A higher C_{na} can also
424 be observed when the initial concentration is increased as to be expected (Figure 4 c).

425 The fragmentation variable, *r* was also varied to test the effect of the breakage function of
426 foods on C_{na}. It can observed from Figure 4 d that the larger the *r* value, the higher the $C_{na,}$
427 although the difference between the other *r* values is not obvious. A larger *r* value
428 corresponds to a higher degree of fragmentation (van der Glas et al., 1987). Therefore, a
429 larger *r* value will produce a higher number of smaller daughter particles. Theoretically, a
430 higher C_{na} should be observed with a larger *r* value as the increase in the number of smaller
431 particles will have created more surface area, resulting to a faster release and movement of
432 the aroma compounds from the rice matrix into the saliva and vapour phases (How et al.,
433 2021).

434 The reason why a less obvious trend (between the three *r* values used in the sensitivity
435 analysis) was observed could be due to the assumption of an entirely constant P value (Eq.
436 10), during chewing, which is a limitation of the study. When *r* and *p* values from Table 1 are
437 plotted (data not shown) against each other, it was shown that they are highly correlated (R^2

438 > 0.9), therefore any change in *r* must be accompanied by a subsequent change of *p* in the
439 same direction because of their causal relationship. By artificially breaking the causal
440 relationship, the effect of an increase of *r* is penalised by a constant value of *p* (which is too
441 small (Table 1) for the increased *r*), while a decrease in *r* is favoured by a constant, too large
442 value of *p*, which produces an artificial reverse effect of modifying *r* separately.

443 As expected, the magnitude of C_{na} is higher when *p* is larger, consistent with the main model
444 assumption (Figure 4 g). It is also expected that increasing *p* gives an expected increasing
445 effect on C_{na} because increasing *p* while keeping *r* constant also mimics the effect of
446 involving more particle sizes above the tiny ones (≤ 0.335 mm; sizes up to 1 mm) in aroma
447 release (Figure 2). Because of the limitation of Eq. 10, it is challenging to postulate the real
448 effect of *r* and *p* parameters on aroma release, without the need to develop a different model
449 that accounts for the strong causal relationship. The development of a new model will include
450 additional experiments to be able to better understand the specific nature and strength of the
451 causal relationship, which is subjected to future studies.

452 The higher the saliva flow rate (represented by the rate constant of the bolus saliva content
453 data), the smaller the magnitude of C_{na} (Figure 4 e), which is to be expected due to the
454 renewal of fresh saliva present in the mouth and pharynx (Doyennette et al., 2014). The
455 volume of saliva also determines the bolus saturation, which is a parameter required to
456 calculate the bolus surface area. A higher salivary flow rate will result in the bolus reaching
457 saturation faster, therefore may decrease surface area of the bolus. This results to a slower
458 rate of transfer of aroma from the bolus to the air phase of the mouth, hence, explains the
459 smaller C_{na} value. Thus, a food manufacturer may avoid adding additional
460 chemical/components (such as citric acid) that may increase the saliva flow rate during
461 mastication. The same trend can also be observed when the initial volume of liquid in the
462 mouth is varied, where a higher initial liquid volume results to a smaller magnitude of C_{na}

(Figure 4 f). This is to demonstrate when rice is served with liquid such as curries or soup which will reach bolus saturation immediately and will therefore have smaller bolus surface area. Finally, it is also interesting to test the effect of the chewing rate on C_{na} as it is dependent on the food structure (e.g., soft vs hard foods). Comparing the magnitude of C_{na} in the first 15 seconds in Figure 4 h, chewing faster has a higher magnitude as it takes a shorter time to swallow for the same initial mass of aroma compounds.

Besides the product, aroma release is also influenced by the physiological parameters of humans. This is a challenge for food technologists as humans show wide variation in these parameters and in the way they consume food (Taylor, 2002). Mathematical modelling can provide insights into understanding the role of individual physiological parameters as these parameters are defined in the model to predict aroma release. In this way, the model can be a tool to design food that can tailor to individual's physiological characteristics.

5.3 Effect of physiological parameters on model predictions

The physiological parameters that are used as the model inputs were manipulated to observe its effects on the aroma release predictions. As can be seen from Figure 5, it can be observed that aroma release was mostly impacted from the breathing frequency, the volume of pharynx, the volume of oral cavity and the volume of nasal cavity while the rest of the parameters seem to have a negligible effect. A higher breathing frequency seems to have lower aroma concentration as it increases the removal of the aroma compound from the mouth. A higher aroma concentration is also observed with a larger oral cavity and it becomes more apparent towards the later stages of mastication. A larger volume of oral cavity indicates a larger volume of aroma-rich air in the oral cavity. Due to this, a higher concentration of aroma will be observed in the nasal cavity as it takes longer for the aroma-rich air in the oral cavity to be depleted during breathing (for the same breath flow rate). The variation of the volume of pharynx gives a higher C_{na} when the volume is smaller. The same

trend can be observed with the variation of the volume of nasal cavity. The effects can be explained from the combination of an aroma-rich air from the oral cavity/pharynx with aroma-free ambient air while breathing. A lower pharynx/nasal cavity volume implies higher renewal rate, therefore it leads to a quicker increase and decrease of the aroma concentration (Trelea et al., 2007). The remaining physiological parameters as seen in Figure 5 seem to have negligible effect on the simulated nasal aroma concentration. This indicates that their accurate knowledge of the parameters is not vital for running the model.

The substantial effects of some of the physiological parameters on aroma concentration can provide knowledge to food manufacturers to design foods to a specific class of consumer. For example, race and gender and known to be the important factors affecting the oral and nasal structures (Xue & Hao, 2006). A study by Xue & Hao (2006) compared the vocal tract dimensions of 120 healthy adult subjects with equal numbers of men and women of three races (White American, African American and Chinese). The results showed that the men have a larger vocal tract dimension (e.g. oral and pharynx volume) compared to women. Chinese people seem to have the largest oral and pharynx volume, followed by White American and African American. Thus, the physiological parameters of the subjects need to be considered by a food manufacturer in the food designing process. If a subject possesses a large oral volume, perhaps only a small initial concentration of aroma compound is required in the food to be able to perceive the 'right amount of flavor'. However, besides the physiological parameters, it is also known that other factors such as the nature of the food matrix and physicochemical factors can affect aroma release. It can be challenging to identify the parameters that have the most effect on a subject through a series of lab experiments as these are time-consuming and financially expensive. Therefore, development of mechanistic models linking oral processing and aroma release provides tools

to explore these interactions and can lead to the development of foods influencing sensorial and digestive outcomes.

5.4 Effect of physico-chemical parameters on model predictions

Physico-chemical factors such as partitioning, interfacial mass transport and diffusion are mechanisms that can affect aroma release (Taylor, 2002). Food technologist is interested in this area as upon mastication, flavour components are released, and the overall sensory appreciation is influenced by the way the components are distributed over the different phases (that make up the food microstructure) and the diffusion kinetics of flavor release and transport of the volatiles to the olfactory epithelium in the nasal cavity (Bruin, 1999).

As can be seen from Figure 6, almost all the physico-chemical parameters have negligible effect on the simulated aroma concentration in the nasal cavity except the mass transfer coefficient of saliva in the oral cavity. A higher aroma concentration is observed with higher value of mass transfer coefficient. This parameter was also pointed out to be one of the key factors governing the release of aroma compounds when a sensitivity analysis was carried out in the aroma release mechanistic model developed for cheese (Doyennette et al., 2014). The mass transfer coefficient could be influenced by the viscosity of the saliva and the stirring rate (tongue and cheek movements), both of which determine the thickness of the stagnant layer (Nahon et al., 2000). Increasing the viscosity of the surrounding fluid by addition of thickeners of simply raising the concentration of aroma in the saliva will therefore decrease the mass transfer coefficient and the rate of flavour release (Nahon et al., 2000). The rest of the physico-chemical parameters such as the partition coefficients (saliva to rice, air to saliva) and the mass transfer coefficients in all physiological compartments all seem to have a negligible effect on the aroma concentration, which indicate that their accurate knowledge is not essential to run the model.

6. Conclusions

An integrated selection-breakage model was coupled with mass transport models to predict aroma release during the consumption of cooked white rice. The validity of the model was tested by comparing model predictions against *in vivo* aroma release data of five subjects. Among the product related parameters studied, the model showed that the portion size, initial concentration of aroma, initial liquid volume and the pasted fraction have the most impact on the aroma concentration. Physiologically, the model showed that the oral cavity volume, pharynx volume, nasal cavity volume and the breathing frequency were the variables that affect aroma concentration the most. The mass transfer coefficient of saliva has the most significant effect on the aroma release among all physico-chemical parameters studied in the model. The effects of the partition coefficient of different aroma compounds were also explored where aromas that had the highest affinity in air showed the highest aroma release. All in all, the incorporation of the mechanistic chewing model in this study provides the first step upon the development of mechanistic models that can lead to the development of foods to influence sensorial and digestive outcomes.

CRediT authorship contribution statement

Syahmeer How: Conceptualization, Methodology, Investigation, Visualization, Formal analysis, Funding acquisition, Writing - original draft. **Jim R. Jones:** Supervision, Visualization, Writing - review & editing. **Marco P. Morgenstern:** Supervision, Writing - review & editing. **Eli Gray-Stuart:** Supervision. **John E. Bronlund:** Supervision, Funding acquisition, Visualization, Formal analysis, Writing - review & editing. **Anne Saint-Eve:** Formal analysis. **Ioan Cristian Trelea:** Visualization, Writing - review & editing. **Isabelle Souchon:** Conceptualization, Methodology, Supervision, Formal analysis, Funding acquisition.

Declaration of competing interest

The authors declare they have no competing interest.

Acknowledgements

The authors would like to acknowledge Riddet Institute CoRE New Zealand (Project 2.b: Physical processes underlying digestion), INRAE and AgroParisTech France for their financial support to carry out the research work in Grignon, France. Syahmeer How is also grateful to the funding provided by Universiti Putra Malaysia (GP-IPM: Grant number: 9712600) to complete the research work. The authors would also like to thank the anonymous reviewers for their valuable comments and suggestions to improve the manuscript.

References

Atlan, S., Trelea, I. C., Saint-Eve, A., Souchon, I., & Latrille, E. (2006). Processing gas chromatographic data and confidence interval calculation for partition coefficients determined by the phase ratio variation method. *Journal of Chromatography A*, *1110*(1-2), 146-155.

Austin, L.G. (1971): A Review: Introduction to the Mathematical Description of Grinding as Rate Process, *Powder Technology*, *5*, 1-17.

Bruin, S. (1999). Phase equilibria for food product and process design Invited lecture, 8th International Conference on Properties and Phase Equilibria for Product and Process Design, April 26–May 1, 1998, Noordwijkerhout, The Netherlands.1. *Fluid Phase Equilibria*, *158-160*, 657-671.

Doyennette, M., de Loubens, C., Deleris, I., Souchon, I., Trelea, I.C. (2011) Mechanisms explaining the role of viscosity and post-deglutitive pharyngeal residue on in vivo aroma release: A combined experimental and modeling study. *Food Chemistry*, *128* (2), 380-390

Doyennette, M., Déléris, I., Féron, G., Guichard, E., Souchon, I., & Trelea, I.C. (2014). Main individual and product characteristics influencing in-mouth flavour release during eating masticated food products with different textures: Mechanistic modelling and experimental validation. *Journal of Theoretical Biology, 340*, 209-221

591 Déléris, I., Saint-Eve, A., Saglio, A., Souchon, I., Trelea, I.C. (2016) Insights in aroma
592 compound retention by mucosa during consumption through mathematical modelling.
593 *Journal of Food Engineering, 190*, 123-138.

594 German, R. M. (2016). Sintering Trajectories: Description on How Density, Surface Area,
595 and Grain Size Change. *JOM*, *68*(3), 878-884.

596 Gray-Stuart, E. M. (2016). *Modelling food breakdown and bolus formation during*
597 *mastication*, Massey University, New Zealand (Doctoral dissertation).
598 https://mro.massey.ac.nz/handle/10179/9859

599 Harrison, M., Campbell, S., & Hills, B. P. (1998). Computer Simulation of Flavor Release
600 from Solid Foods in the Mouth. *Journal of Agricultural and Food Chemistry*, *46*(7),
601 2736-2743.

602 Harrison, S. M., & Cleary, P. W. (2014). Towards modelling of fluid flow and food breakage
603 by the teeth in the oral cavity using smoothed particle hydrodynamics (SPH).
604 *European Food Research and Technology*, *238*(2), 185-215.

605 How, M. S., Jones, J. R., Morgenstern, M. P., Gray-Stuart, E., Bronlund, J. E., Saint-Eve, A.,
606 ... & Souchon, I. (2021). Modelling the role of oral processing on in vivo aroma
607 release of white rice: Conceptual model and experimental validation. *LWT*, *141*,
608 110918.

609 How, M. S., Jones, J. R., Morgenstern, M. P., Gray-Stuart, E., & Bronlund, J. E. (2022). A
610 mechanistic approach to model the breakdown of solid food during chewing. *Journal*
611 *of Food Engineering*, *317*, 110871.

Kantono, K., How, M. S., & Wang, Q. J. (2022). Design of experiments meets immersive environment: Optimising eating atmosphere using artificial neural network. *Appetite*, 106122.

Le Révérend, B. J., Norton, I. T., & Bakalis, S. (2013). Modelling the human response to saltiness. *Food & Function, 4*(6), 880-888.

Matsuo, K., Metani, H., Mays, K. A., & Palmer, J. B. (2010). Effects of respiration on soft palate movement in feeding. *Journal of Dental Research, 89*(12), 1401-1406. 10.1177/0022034510377336

Ming, J. L. K., Anuar, M. S., How, M. S., Noor, S. B. M., Abdullah, Z., & Taip, F. S. (2021). Development of an Artificial Neural Network Utilizing Particle Swarm Optimization for Modeling the Spray Drying of Coconut Milk. *Foods*, *10*(11), 2708.

Mohd Firdaus How, M. S. H. (2021). *Modelling of chewing and aroma release during oral processing: model development, model validation and comprehensive examples for food design: a thesis presented in partial fulfilment of the requirements for the degree of Doctor of Philosophy in Chemical and Bioprocess Engineering, Massey University, Palmerston North, New Zealand* (Doctoral dissertation, Massey University). https://mro.massey.ac.nz/handle/10179/16525

Motoi, L., Morgenstern, M. P., Hedderley, D. I., Wilson, A. J., & Balita, S. (2013). Bolus Moisture Content of Solid Foods during Mastication. *Journal of Texture Studies, 44*(6), 468-479.

Nahon, D. F., Harrison, M., & Roozen, J. P. (2000). Modeling flavor release from aqueous sucrose solutions, using mass transfer and partition coefficients. *Journal of Agricultural and Food Chemistry, 48*(4), 1278-1284.

635 Rabe, S., Krings, U., & Berger, R. G. (2004). Dynamic flavour release from Miglyol/water
636 emulsions: modelling and validation. *Food Chemistry*, *84*(1), 117-125.

637 Taylor, A. J. (2002). Release and Transport of Flavors In Vivo: Physicochemical,
638 Physiological, and Perceptual Considerations. *Comprehensive Reviews in Food*
639 *Science and Food Safety*, *1*(2), 45-57.

640 Trelea, I.C., Atlan, S., Déléris, I., Saint-Eve, A., Marin, M., Souchon, I. (2008) Mechanistic
641 mathematical model for in vivo aroma release during eating of semiliquid foods.
642 *Chemical Senses*, *33* (2),181-192

643 van der Bilt, A., van der Glas, H. W., Olthoff, L. W., & Bosman, F. (1991). The effect of
644 particle size reduction on the jaw gape in human mastication. *Journal of Dental*
645 *Research*, *70*(5), 931-937.

646 van der Bilt, A., Olthoff, L. W., van der Glas, H. W., van der Weelen, K., & Bosman, F.
647 (1987). A mathematical description of the comminution of food during mastication in
648 man. *Archives of Oral Biology*, *32*(8), 579-586.

649 van der Glas, H. W., van der Bilt, A., Olthoff, L. W., & Bosman, F. (1987). Measurement of
650 Selection Chances and Breakage Functions During Chewing in Man. *Journal of*
651 *Dental Research*, *66*(10), 1547-1550.

652 van der Glas, H. W., van der Bilt, A., & Bosman, F. (1992). A selection model to estimate the
653 interaction between food particles and the post-canine teeth in human mastication.
654 *Journal of Theoretical Biology*, *155*(1), 103-120.

655 van der Glas, H. W., Kim, E. H. J., Mustapa, A. Z., & Elmanaseer, W. R. (2018). Selection in
656 mixtures of food particles during oral processing in man. *Archives of Oral Biology*,
657 *85*, 212-225.

Wright, K. M., Sprunt, J., Smith, A. C., & Hills, B. P. (2003). Modelling flavour release from a chewed bolus in the mouth: Part I. Mastication. *International journal of food science & technology*, *38*(3), 351-360.

Xue, S. A., & Hao, J. G. (2006). Normative Standards for Vocal Tract Dimensions by Race as Measured by Acoustic Pharyngometry. *Journal of Voice, 20*(3), 391-400.

Yu, L., Witt, T., Bonilla, M. R., Turner, M. S., Fitzgerald, M., & Stokes, J. R. (2019). New insights into cooked rice quality by measuring modulus, adhesion and cohesion at the level of an individual rice grain. *Journal of Food Engineering*, *240*, 21-28.

Zhang, Y., Jia, J., Wang, X., Chen, J., & van der Glas, H. W. (2021). Particle size distributions following chewing: Transformation of two-dimensional outcome from optical scanning to volume outcome from sieving. *Journal of Food Engineering*, *309*, 110663.

List of Figure Captions

Figure 1. Conceptual diagram of the interconnected compartments and the mechanisms involved in flavour release during the consumption of cooked white rice.

Figure 2. Best-fit model against experimental data for Subject A4. Two-way interaction model was used as the selection model. The plot on the left of the image is the comparison of the d-values of the best fit model and the experimental data whereas the plot on the right shows the comparison of the pasted fraction values. The error-bar of the model is the standard deviation of 50 simulations. All 3 replicates of the measured data (three different markers) were plotted for comparison.

Figure 3. Model prediction against experimental data of 2-nonanone (m/z 143) and ethyl propanoate (m/z 103) for Subject A4. Rel. AUC refers to the relative cumulative area under the curve, where the cumulative area under the curve was normalised against the total area under the curve.The model was also predicted using different pasted size threshold (0.2 mm, 0.354 mm, 1 mm and when all particles were pasted) and compared against the five replicates of the experimental data.

Figure 4. Effect of parameters related to the product and individual which may be of interest to a food manufacturer. Using the physiological parameters of Subject A4, C_{na} of 2-nonanone was predicted.a. Aroma release (C_{na}) when portion size is varied (2.5 g, 5 g and 10 g of rice), b. Aroma release (C_{na}) when initial particle size is varied (halved, original and doubled size) for 5 g of rice c. Aroma release (C_{na}) when the initial concentration is varied for 5 g of rice, d. Aroma release (C_{na}) when the breakage function (represented by the fragmentation variable, r) is varied for 5 g of rice, e. Aroma release (C_{na}) when saliva flow rate is varied for 5 g of rice, f. Aroma release (C_{na}) when the initial liquid volume iis varied for 5 g of rice, g. Aroma release (C_{na}) when the breakage function (represented by the pasted fraction, p) is varied for 5 g of rice, h. Aroma release (C_{na}) when the chewing rate (0.7 chew/s, 1.5 chew/s and 2 chew/s) is varied for 5 g of rice

Figure 5. Effect of physiological parameters on aroma release (C_{na}). Using the physiological parameters of Subject A4 as a reference value, C_{na} of 2-nonanone was predicted. a. Effect of breathing frequency on aroma release (C_{na}) (0.12 cycle/s, 0.25 cycle/s, 0.32 cycle/s), b. Effect of the oral cavity volume on aroma release (C_{na}) (2×10^{-5} m^3, 6×10^{-5} m^3, 1×10^{-4} m^3) c. Effect of the pharynx volume on aroma release (C_{na}) (1.5×10^{-5} m^3, 3.2×10^{-5} m^3, 6×10^{-5} m^3mm^3), d. Effect of the nasal cavity volume on aroma release (C_{na}) (1.2×10^{-5} m^3, 1.6×10^{-5} m^3, 4×10^{-5} m^3), e. Effect of the oral mucosa thickness on aroma release (C_{na}) (5×10^{-6} m, 5×10^{-5} m, 5×10^{-4} m), f. Effect of the pharynx mucosa thickness on aroma release (C_{na}) (5×10^{-6} m, 5×10^{-5} m, 5×10^{-4} m), g. Effect of the nasal mucosa thickness on aroma release (C_{na}) (5×10^{-6} m, 5×10^{-5} m, 5×10^{-4} m), h. Effect of tidal volume on aroma release (C_{na}) (2.5×10^{-4} m^3, 5×10^{-4} m^3, 1×10^{-3} m^3), i. Effect of oral cavity area on aroma release (C_{na}) (5.8×10^{-3} m^2, 1.6×10^{-2} m^2, 2.32×10^{-2} m^2), j. Effect of pharynx area on aroma release (C_{na}) (3.3×10^{-3} m^2, 6.5×10^{-3} m^2, 1.3×10^{-2} m^2), k. Effect of air/mucosa contact area in the nasal cavity on aroma release (C_{na}) (7.5×10^{-3} m^2, 1.6×10^{-2} m^2, 3×10^{-2} m^2), l. Effect of volume of saliva in pharynx (C_{na}) (1×10^{-7} m^3, 1×10^{-7} m^3, 4×10^{-7} m^3)

Figure 6. Effect of physico-chemical parameters on aroma release (C_{na}). Using the physiological parameters of Subject A4 as a reference value, C_{na} of 2-nonanone was predicted. a. Effect of saliva/rice partition coeffcient on aroma release (C_{na}) (2.45×10^{-2}, 2.45×10^{-1},2.45), b. Effect of air/saliva partition coefficient on aroma release (C_{na}) (9.7×10^{-4}, 9.7×10^{-3}, 9.7×10^{-2}) c. Effect of air/mucosa partition coefficient in the oral cavity on aroma release (C_{na}) (1×10^{-5}, 1×10^{-3}, 1×10^{-1}), d Effect of air/mucosa partition coefficient in the pharynx on aroma release (C_{na}) (1×10^{-5}, 1×10^{-3}, 1×10^{-1}), e. Effect of air/mucosa partition coefficient in the nasal cavity on aroma release (C_{na}) (1×10^{-5}, 1×10^{-3}, 1×10^{-1}), f. Effect of air/saliva partition coefficient in the pharynx on aroma release (C_{na}) (5×10^{-4}, 5×10^{-3}, 5×10^{-2}), g. Effect of mass transfer coefficient in saliva in oral cavity on aroma release (C_{na}) (1×10^{-8} m/s, 1×10^{-6} m/s, 1×10^{-4} m/s), h. Effect of mass transfer coefficient in saliva in pharynx on aroma release (C_{na}) (1×10^{-8} m/s, 1×10^{-6} m/s, 1×10^{-4} m/s), i. Effect of mass transfer coefficient in mucosa in oral cavity on aroma release (C_{na}) (1×10^{-8} m/s, 1×10^{-6} m/s, 1×10^{-4} m/s), j. Effect of mass transfer coefficient in mucosa in pharynx on aroma release (C_{na}) (1×10^{-8} m/s, 1×10^{-6} m/s, 1×10^{-4} m/s) , k. Effect of mass transfer coefficient in mucosa in nasal cavity on aroma release (C_{na}) (1×10^{-8} m/s, 1×10^{-6} m/s, 1×10^{-4} m/s)

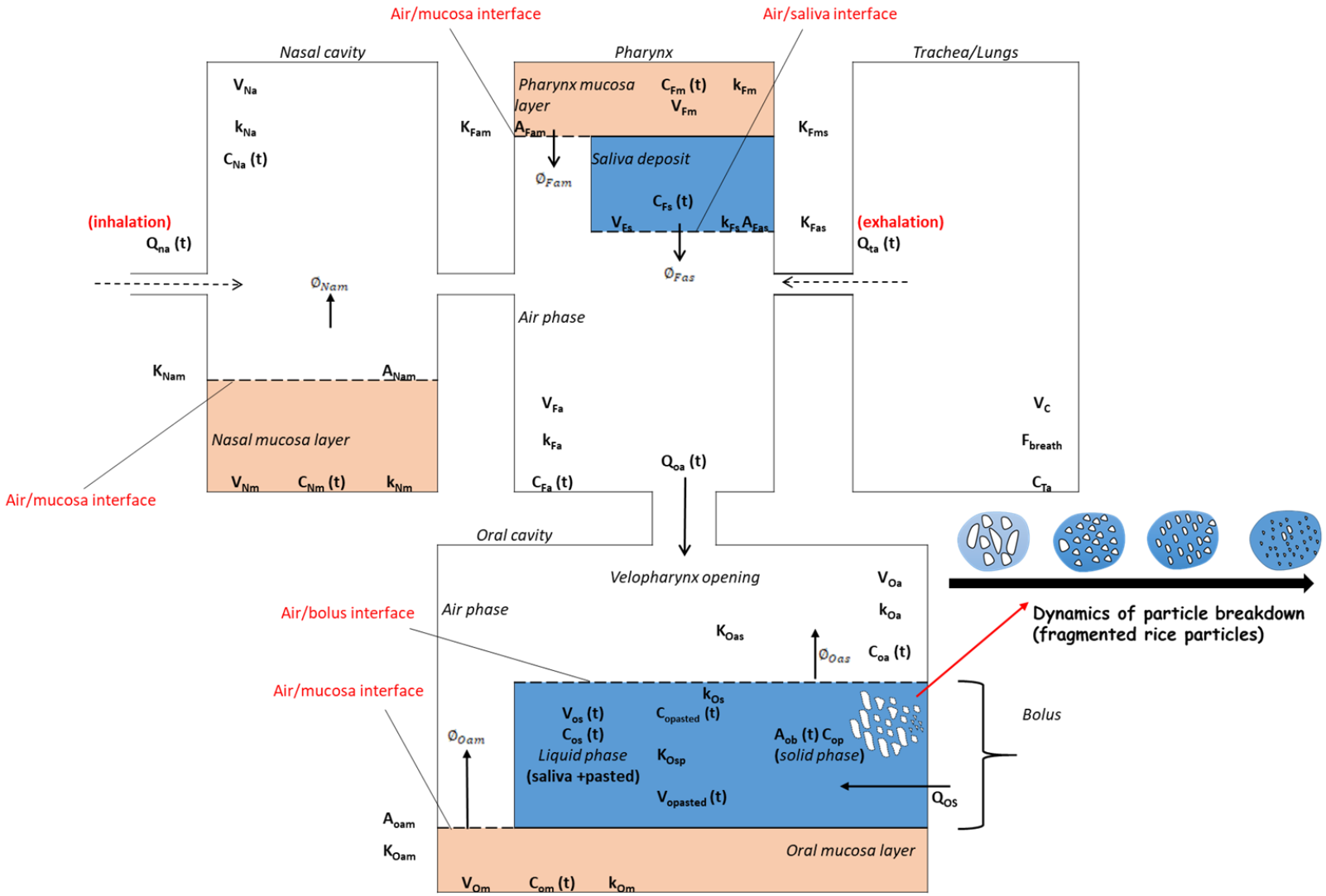

Figure 1. Conceptual diagram of the interconnected compartments and the mechanisms involved in flavour release during the consumption of cooked white rice.

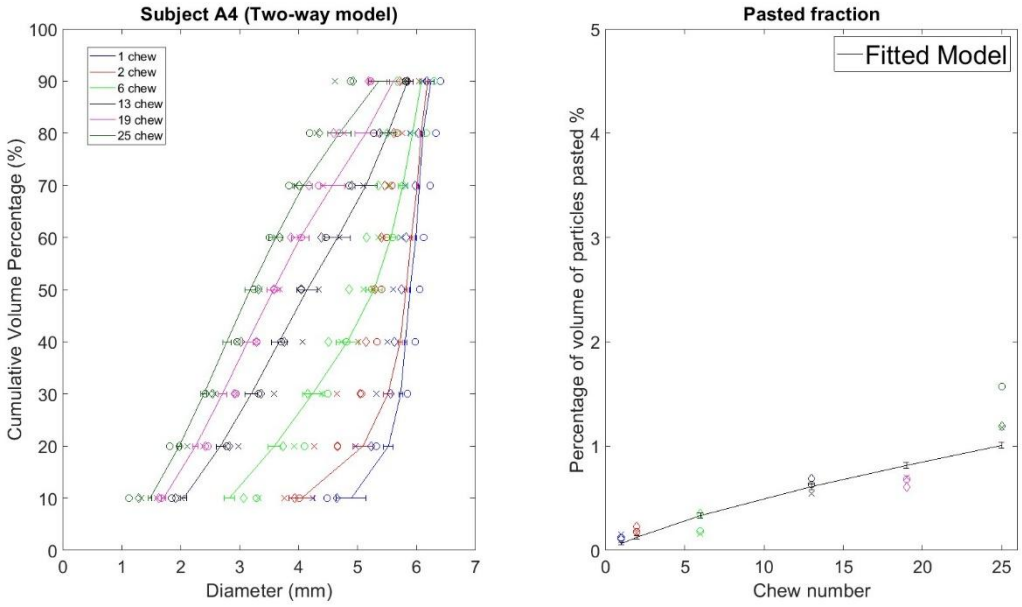

Figure 2. Best-fit model against experimental data for Subject A4. Two-way interaction model was used as the selection model. The plot on the left of the image is the comparison of the d-values of the best fit model and the experimental data whereas the plot on the right shows the comparison of the pasted fraction values. The error-bar of the model is the standard deviation of 50 simulations. All 3 replicates of the measured data (three different markers) were plotted for comparison.

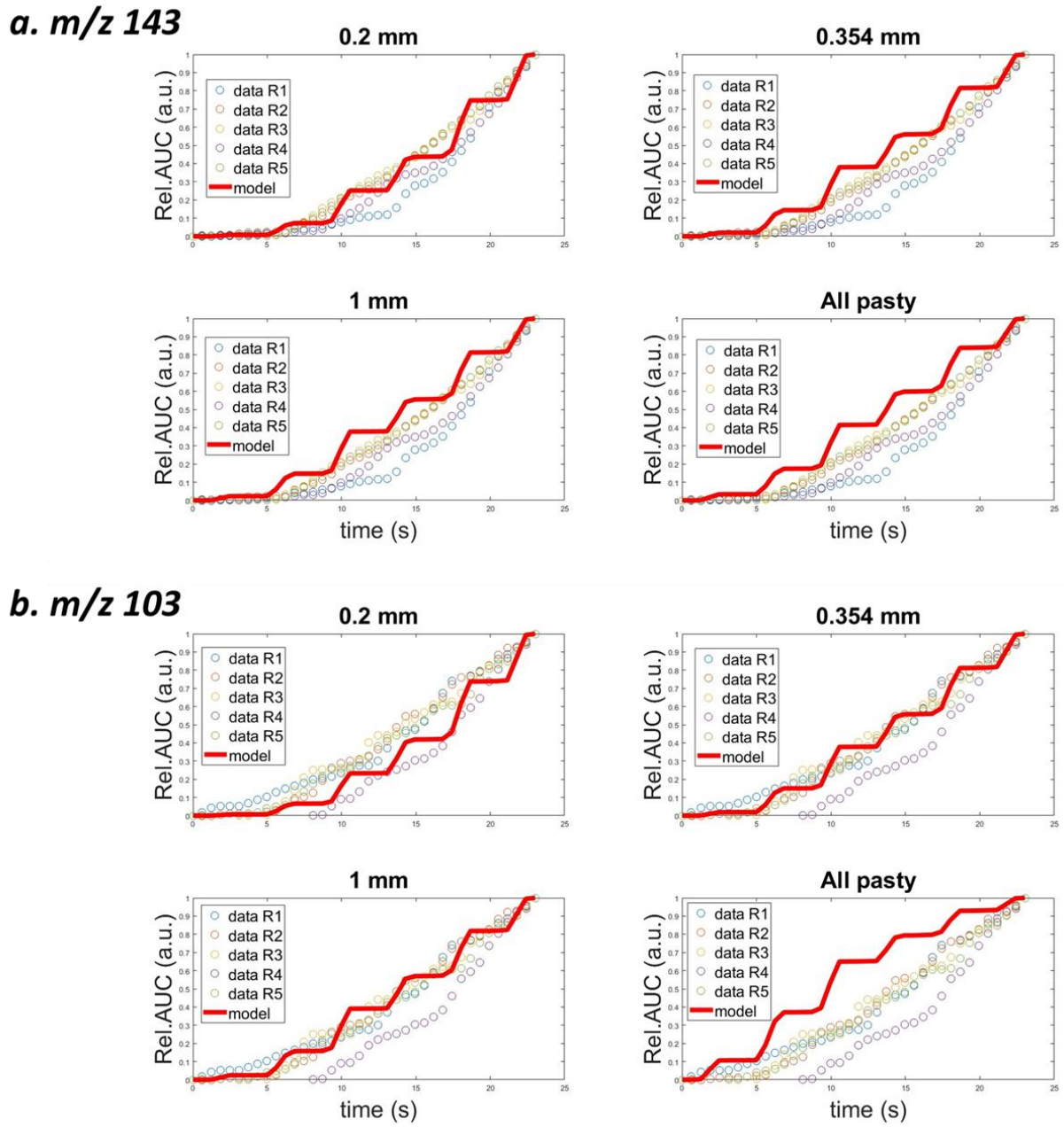

Figure 3. Model prediction against experimental data of 2-nonanone (m/z 143) and ethyl propanoate (m/z 103) for Subject A4. Rel. AUC refers to the relative cumulative area under the curve, where the cumulative area under the curve was normalised against the total area under the curve.The model was also predicted using different pasted size threshold (0.2 mm, 0.354 mm, 1 mm and when all particles were pasted) and compared against the five replicates of the experimental data.

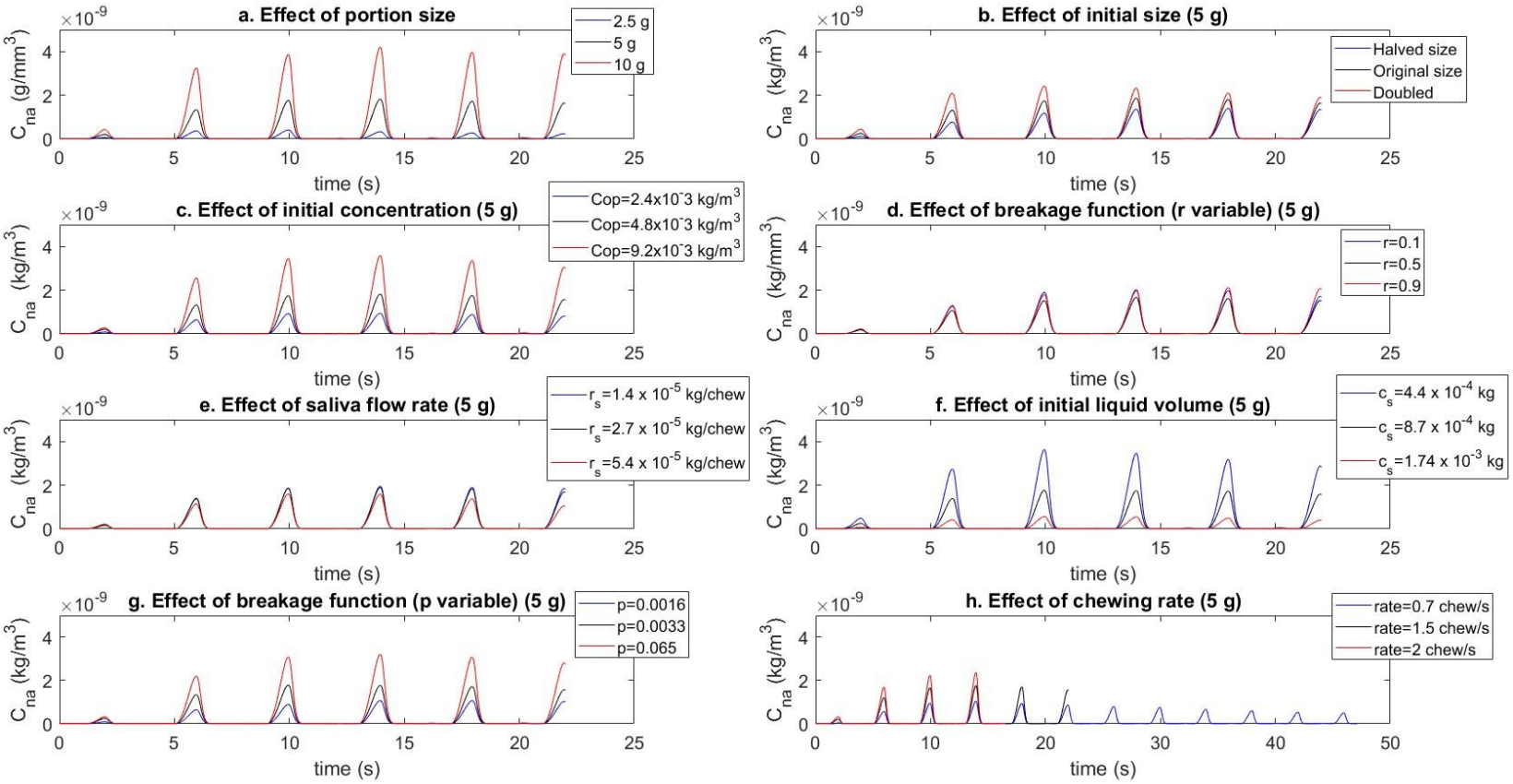

Figure 4. Effect of parameters related to the product and individual which may be of interest to a food manufacturer. Using the physiological parameters of Subject A4, C_{na} of 2-nonanone was predicted.a. Aroma release (C_{na}) when portion size is varied (2.5 g, 5 g and 10 g of rice), b. Aroma release (C_{na}) when initial particle size is varied (halved, original and doubled size) for 5 g of rice c. Aroma release (C_{na}) when the initial concentration is varied for 5 g of rice, d. Aroma release (C_{na}) when the breakage function (represented by the fragmentation variable, r) is varied for 5 g of rice, e. Aroma release (C_{na}) when saliva flow rate is varied for 5 g of rice, f. Aroma release (C_{na}) when the initial liquid volume iis varied for 5 g of rice, g. Aroma release (C_{na}) when the breakage function (represented by the pasted fraction, p) is varied for 5 g of rice, h. Aroma release (C_{na}) when the chewing rate (0.7 chew/s, 1.5 chew/s and 2 chew/s) is varied for 5 g of rice

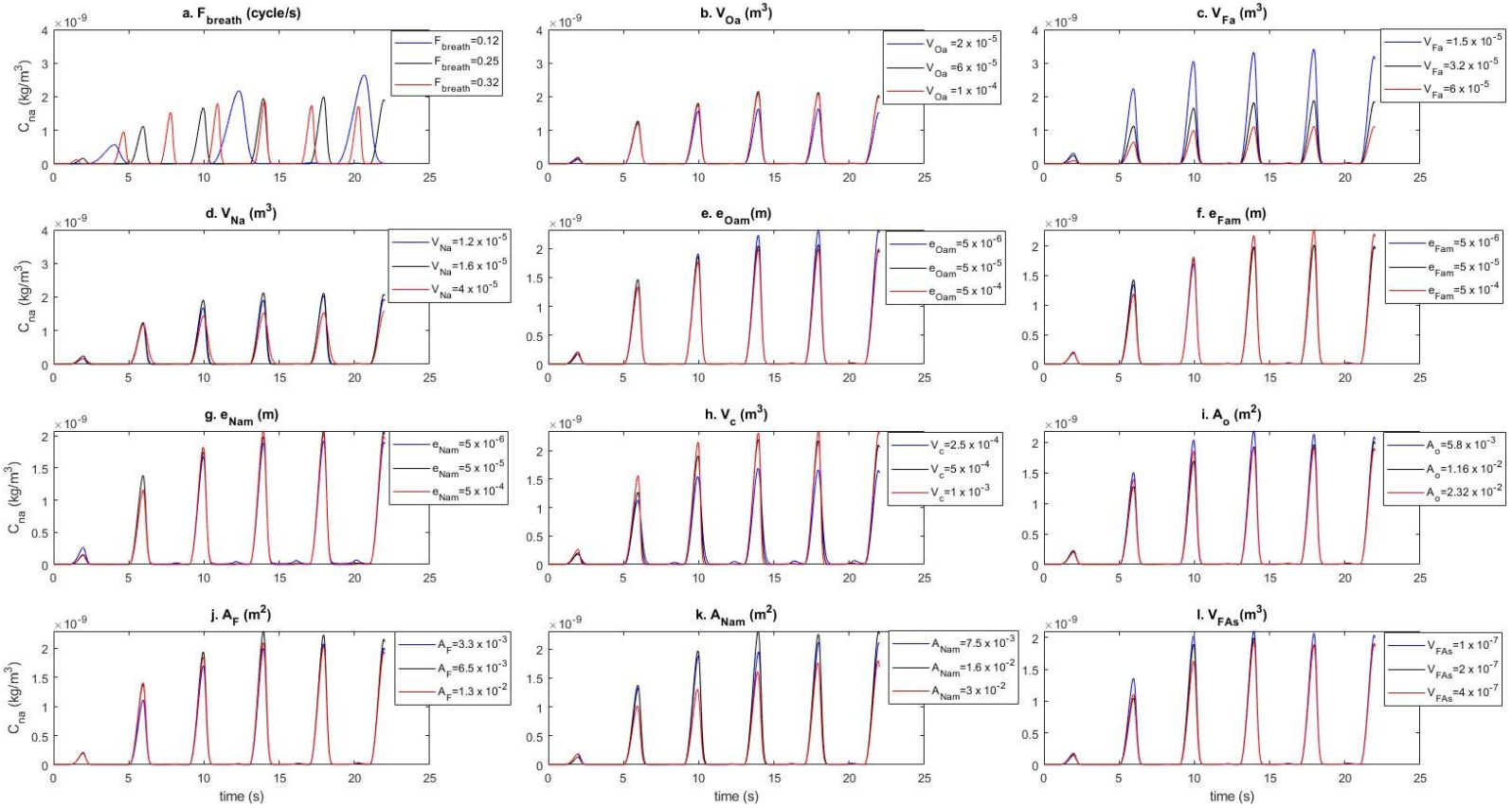

Figure 5. Effect of physiological parameters on aroma release (C_{na}). Using the physiological parameters of Subject A4 as a reference value, C_{na} of 2-nonanone was predicted. a. Effect of breathing frequency on aroma release (C_{na}) (0.12 cycle/s, 0.25 cycle/s, 0.32 cycle/s), b. Effect of the oral cavity volume on aroma release (C_{na}) (2×10^{-5} m^3, 6×10^{-5} m^3, 1×10^{-4} m^3) c. Effect of the pharynx volume on aroma release (C_{na}) (1.5×10^{-5} m^3, 3.2×10^{-5} m^3, 6×10^{-5} m^3mm^3), d. Effect of the nasal cavity volume on aroma release (C_{na}) (1.2×10^{-5} m^3, 1.6×10^{-5} m^3, 4×10^{-5} m^3), e. Effect of the oral mucosa thickness on aroma release (C_{na}) (5×10^{-6} m, 5×10^{-5} m, 5×10^{-4} m), f. Effect of the pharynx mucosa thickness on aroma release (C_{na}) (5×10^{-6} m, 5×10^{-5} m, 5×10^{-4} m), g. Effect of the nasal mucosa thickness on aroma release (C_{na}) (5×10^{-6} m, 5×10^{-5} m, 5×10^{-4} m), h. Effect of tidal volume on aroma release (C_{na}) (2.5×10^{-4} m^3, 5×10^{-4} m^3, 1×10^{-3} m^3), i. Effect of oral cavity area on aroma release (C_{na}) (5.8×10^{-3} m^2, 1.6×10^{-2} m^2, 2.32×10^{-2} m^2), j. Effect of pharynx area on aroma release (C_{na}) (3.3×10^{-3} m^2, 6.5×10^{-3} m^2, 1.3×10^{-2} m^2), k. Effect of air/mucosa contact area in the nasal cavity on aroma release (C_{na}) (7.5×10^{-3} m^2, 1.6×10^{-2} m^2, 3×10^{-2} m^2), l. Effect of volume of saliva in pharynx (C_{na}) (1×10^{-7} m^3, 1×10^{-7} m^3, 4×10^{-7} m^3)

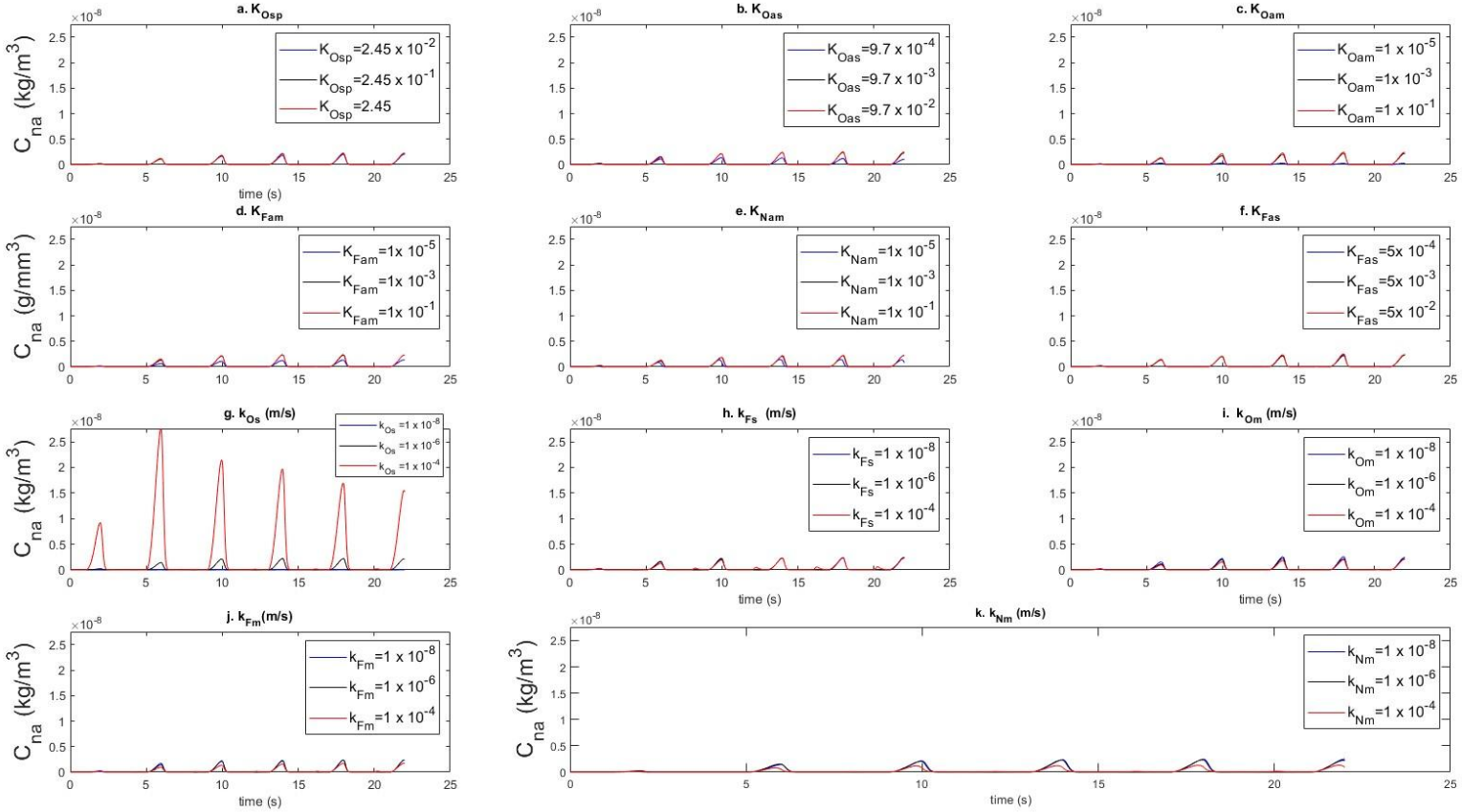

Figure 6. Effect of physico-chemical parameters on aroma release (C_{na}). Using the physiological parameters of Subject A4 as a reference value, C_{na} of 2-nonanone was predicted. a. Effect of saliva/rice partition coeffcient on aroma release (C_{na}) (2.45×10^{-2}, 2.45×10^{-1},2.45), b. Effect of air/saliva partition coefficient on aroma release (C_{na}) (9.7×10^{-4}, 9.7×10^{-3}, 9.7×10^{-2}) c. Effect of air/mucosa partition coefficient in the oral cavity on aroma release (C_{na}) (1×10^{-5}, 1×10^{-3}, 1×10^{-1}), d Effect of air/mucosa partition coefficient in the pharynx on aroma release (C_{na}) (1×10^{-5}, 1×10^{-3}, 1×10^{-1}), e. Effect of air/mucosa partition coefficient in the nasal cavity on aroma release (C_{na}) (1×10^{-5}, 1×10^{-3}, 1×10^{-1}), f. Effect of air/saliva partition coefficient in the pharynx on aroma release (C_{na}) (5×10^{-4}, 5×10^{-3}, 5×10^{-2}), g. Effect of mass transfer coefficient in saliva in oral cavity on aroma release (C_{na}) (1×10^{-8} m/s, 1×10^{-6} m/s, 1×10^{-4} m/s), h. Effect of mass transfer coefficient in saliva in pharynx on aroma release (C_{na}) (1×10^{-8} m/s, 1×10^{-6} m/s, 1×10^{-4} m/s), i. Effect of mass transfer coefficient in mucosa in oral cavity on aroma release (C_{na}) (1×10^{-8} m/s, 1×10^{-6} m/s, 1×10^{-4} m/s), j. Effect of mass transfer coefficient in mucosa in pharynx on aroma release (C_{na}) (1×10^{-8} m/s, 1×10^{-6} m/s, 1×10^{-4} m/s) , k. Effect of mass transfer coefficient in mucosa in nasal cavity on aroma release (C_{na}) (1×10^{-8} m/s, 1×10^{-6} m/s, 1×10^{-4} m/s)

List of Table Captions

Table 1. Best fit input parameters of the PSD model evaluated from the PSO algorithm. The two-way competition selection model was applied integrated with a constant breakage model (Eq.10). The R-squared value was given to describe the goodness of fit.

Table 1. Best fit input parameters of the PSD model evaluated from the PSO algorithm. The two-way competition selection model was applied integrated with a constant breakage model (Eq.10). The R-squared value was given to describe the goodness of fit.

Subject	Selection model	Selection model inputs				Breakage model input		Normalised SS residuals	SS	*R-squared*
		Number of breakage sites, n_b		Affinity factor, o_1						
		Multiplication factor, k	*Power, m*	*Multiplication factor, p*	*Power, q*	*Fragmentation variable, r*	*Pasted fraction, p*			
A1	***Two-way competition***	199.83	1.19	0.003	1.58	0.48	0.003	3.69	33.35	0.79
A2	***Two-way competition***	448.14	1.68	0.001	1.98	0.65	0.006	2.54	23.53	0.84
A3	***Two-way competition***	341.5	2.11	0.002	1.69	0.61	0.004	5.07	48.96	0.73
A4	***Two-way competition***	212.42	1.34	0.002	1.96	0.59	0.003	0.95	4.22	0.98
A5	***Two-way competition***	210.22	1.08	0.002	1.35	0.66	0.005	0.83	10.86	0.94

Appendix A1 – List of Nomenclatures

Table A-1 defines the variables used in the model development used in this chapter.

Table A-1 List of nomenclature

Symbol	Unit	Description
A_{Oam}	m^2	air/lubricated mucosa contact area in the oral cavity
A_{Ob}	m^2	air/bolus contact area in the oral cavity
A_{Fas}	m^2	air/saliva contact area in the pharynx
A_{Fam}	m^2	air/lubricated mucosa in the pharynx
A_{Nam}	m^2	air/lubricated mucosa in the nasal cavity
C_{Os}	kg/m^3	aroma concentration in the saliva in the oral cavity
C_{Oa}	kg/m^3	aroma concentration in the air in the oral cavity
C_{Om}	kg/m^3	aroma concentration in the lubricated mucosa in the oral cavity
C_{Op}	kg/m^3	aroma concentration in the product (rice) in the oral cavity
C_{Fs}	kg/m^3	aroma concentration in the saliva in the pharynx
C_{Fa}	kg/m^3	aroma concentration in the air in the pharynx
C_{Fm}	kg/m^3	aroma concentration in the lubricated mucosa in the pharynx
C_{Na}	kg/m^3	aroma concentration in the air in the nasal cavity
C_{Nm}	kg/m^3	aroma concentration in the lubricated mucosa in the nasal cavity
C_{Ta}	kg/m^3	aroma concentration in the trachea
F_{breath}	number of cycles/s	breathing frequency
$fr_{opening}$	occurrence number/s	opening frequency of the velopharynx
fr_{chew}	number of chews/s	chewing frequency
k_{Oa}	m/s	mass transfer coefficient in the air phase in the oral cavity
k_{Os}	m/s	mass transfer coefficient in the saliva phase in the oral cavity
k_{Om}	m/s	mass transfer coefficient in the lubricated mucosa in the oral cavity
k_{Fs}	m/s	mass transfer coefficient in the

		saliva phase in the pharynx
k_{Fa}	m/s	mass transfer coefficient in the air phase in the pharynx
k_{Fm}	m/s	mass transfer coefficient in the lubricated mucosa in the pharynx
k_{Na}	m/s	mass transfer coefficient in the air phase in the nasal cavity
k_{Nm}	m/s	mass transfer coefficient in the lubricated mucosa in the nasal cavity
K_{Oas}		air/saliva partition coefficient in the oral cavity
K_{Oam}		air/lubricated mucosa partition coefficient in the oral cavity
K_{Osp}		saliva/product(rice) partition coefficient in the oral cavity
K_{Fas}		air/saliva partition coefficient in the pharynx
K_{Fms}		lubricated mucosa/saliva partition coefficient in the pharynx
K_{Fam}		air/lubricated mucosa partition coefficient in the pharynx
K_{Nam}		air/lubricated mucosa partition coefficient in the nasal cavity
V_{bolus}	m^3	volume of bolus
V_c	m^3	current breath volume
V_{Os}	m^3	volume of saliva in the oral cavity
V_{Osrest}	m^3	volume of saliva at rest in the oral cavity
$V_{Opasted}$	m^3	volume of pasted rice particles in the oral cavity
V_{Om}	m^3	volume of mucosa in the oral cavity
V_{Oa}	m^3	volume of air in the oral cavity
V_{fluid}	m^3	volume of saliva surrounded on a single particle
V_{Fa}	m^3	volume of air in the pharynx
V_{Fs}	m^3	volume of saliva in the pharynx
V_{Fm}	m^3	volume of mucosa in the pharynx
V_{Na}	m^3	volume of air in the nasal cavity
V_{Nm}	m^3	volume of mucosa in the nasal cavity
V_p	m^3	volume of a single particle

$V_{p\,total}$	m^3	total volume of particles (non-pasted)
V_{tot}	m^3	volume of particle and surrounding saliva
Q_{Os}	m^3/s	saliva flow rate in the oral cavity
Q_{Oa}	m^3/s	air flow rate in the oral cavity
Q_{Na}	m^3/s	air flow rate in the nasal cavity
Q_{Ta}	m^3/s	air flow rate in the trachea
r	m	radius of a particle
R	m	radius of a bolus
S		saturation of the bolus
SA_E	m^2	surface area of expanded bolus
SA_{sphere}	m^2	surface area of a spherical bolus
t	s	time
ϕ		volume fraction of bolus
ϕ_E		volume fraction of expanded bolus
ϕ_{Oas}	kg/s	volatile mass flux between air and saliva in the oral cavity
ϕ_{Oam}	kg/s	volatile mass flux between air and lubricated mucosa in the oral cavity
ϕ_{Fam}	kg/s	volatile mass flux between air and lubricated mucosa in the pharynx
ϕ_{Fas}	kg/s	volatile mass flux between air and saliva in the pharynx
ϕ_{Nam}	kg/s	volatile mass flux between air and lubricated mucosa in the nasal cavity
ε	-	porosity

Appendix A2 – Other equations used to predict aroma release as described in Doyennette et al. (2014)

Air/bolus interfacial conditions in the oral cavity

$$C_{Os}(t) = \frac{C_{Oa}(t)}{K_{Oas}} \#(A2-1)$$

Aroma compound retention by the lubricated mucosa in the oral cavity, pharynx and nasal cavity

$$V_{Om}\frac{dO_m(t)}{dt} = -k_{Om}A_{Oam}\left(C_{Om}(t) - \frac{C_{Oa}(t)}{K_{Oam}}\right) \#(A2-2)$$

Air in the oral cavity

$$V_{Oa\,(t)}\frac{dC_{Oa}(t)}{dt} = A_{Ob}k_{Os}\left(C_{Os}(t) - \frac{C_{Oa}(t)}{K_{Oas}}\right) + k_{Om}A_{Oam}(C_{Om}(t) - \frac{C_{Oa}(t)}{K_{Oam}})$$

$$+\begin{cases} Q_{Oa}(t)\big(C_{Fa}(t) - C_{Oa}(t)\big) & if\ Q_{Oa}(t) \geq 0 \\ 0 & if\ Q_{Oa}(t) < 0 \end{cases}_{\#}$$

.... $(A2-3)$

$$V_{Oa\,(t)} = V_{Oa\,mean} + \Delta V_{Oa}\sin\left(2\pi f r_{opening}t\right) \#(A2-4)$$

$$Q_{Oa}(t) = \frac{dV_{Oa}(t)}{dt}$$

$$= 2\pi f r_{opening}\Delta V_{Oa}\cos(2\pi\, f r_{opening}t) \qquad (A2-5)$$

Bolus in the pharynx

$$V_{Fs}\frac{dC_{Fs}(t)}{dt} = -k_{Fs}A_{Fas}(C_{Fs}(t) - \frac{C_{Fa}(t)}{K_{Fas}}) \ \#(A2-6)$$

Air in the pharynx

$$Q_{Na}(t) = -Q_{Ta}(t) + Q_{Oa}(t) \#(A2-7)$$

$$V_{Fa}\frac{dC_{Fa}(t)}{dt} = k_{Fs}A_{Fas}(C_{Fs}(t) - \frac{C_{Fa}(t)}{K_{Fas}}) + k_{Fm}A_{Fam}\left(C_{Fm}(t) - \frac{C_{Fa}(t)}{K_{Fam}}\right)$$

$$+\begin{cases} -Q_{Oa(t)}(C_{Oa}(t) - C_{Fa}(t)) & if\ Q_{Oa(t)} < 0 \\ Q_{Na(t)}(C_{Na}(t) - C_{Fa}(t)) & if\ Q_{Na(t)} \geq 0 \\ Q_{Ta(t)}(C_{Ta}(t) - C_{Fa}(t)) & if\ Q_{Ta(t)} \geq 0 \end{cases}_{\#}$$

... $(A2-8)$

Air in the nasal cavity

The mass balance of the aroma compound in the air phase in the nasal cavity is given by:

$$V_{Na}\frac{dC_{Na}(t)}{dt} = k_{Nm}A_{Nam}\left(C_{Nm}(t) - \frac{C_{Na}(t)}{K_{Nam}}\right) + \begin{cases} Q_{Na}(t)\,(0 - C_{Na}(t))\ if\ Q_{Na}(t) < 0 \\ Q_{Na}(t)\,(C_{Fa}(t) - C_{Na}(t))\ if\ Q_{Na}(t) \geq 0 \end{cases}$$

$$\#\ldots(A2-9)$$

Appendix A3 – Bolus Surface Area Full Derivation

The following derivation shows the steps required and assumptions made to calculate the bolus surface area.

For example, if each particle is assumed as a sphere (to provide clarity spherical shape is used here but the equations will be adaptable to other particle shape as well), the volume of a particle can be described as

$$V_p = \frac{4}{3}\pi r^3 \#(A3-1)$$

If it was assumed that each particle has an amount of fluid volume, V_{fluid} associated with it, the volume fraction of the fluid with respect to the volume of particle is

$$a = \frac{V_{fluid}}{V_p} \#(A3-2)$$

Therefore the V_{fluid} is

$$V_{fluid} = a\frac{4}{3}\pi r^3 \#(A3-3)$$

Assuming that each particle has an even and the same coating thickness, *x* (independent of size), the total volume of the particle and the fluid can be described as

$$V_{tot} = \frac{4}{3}\pi (r+x)^3 \#(A3-4)$$

where the V_{fluid} can also be calculated by subtracting V_{tot} with V_p. Hence,

$$V_{fluid} = \frac{4}{3}\pi (r+x)^3 - \frac{4}{3}\pi r^3 \#(A3-5)$$

Equating Eq.A3-3 and Eq. A3-5, *x* can be described as

$$x = r(1+a)^3 - r \#(A3-6)$$

Therefore, the surface area of a particle with a coating thickness can be described as

$$A_p = 4\,\pi\,(r + x)^2 \#(A3 - 7)$$

Substituting Eq. A3-6 into Eq. A3-7

$$A_p = 4\,\pi\,r^2(1 + a)^{\frac{2}{3}} \#(A3 - 8)$$

If n_p is the total number of particles, the total surface area of all particles (before they coalescence due to saliva bonding) can be described as

$$4\pi(1 + a)^{\frac{2}{3}} \sum_{i}^{n_p} r_i^2 \,\#(A3 - 9)$$

For the sintering mechanism, a linear relationship was proposed between the surface area and the packing density where the surface area declines as the density increases (German, 2016). Thus, the surface area of a bolus can be described as

$$A_{Ob} = b\emptyset + c \#(A3 - 10)$$

Assuming that the initial packing density is $\emptyset_E$, the initial surface area of the bolus is therefore

$$SA_E = b\emptyset_E + c \#(A3 - 11)$$

Assuming that the bolus forms a perfect sphere when the voidage between particles is 100% saturated with saliva ($\emptyset = 1$), the surface area of the bolus when at 100% saturation is

$$SA_{sphere} = b + c \#(A3 - 12)$$

Substituting Eq A3-12 into Eq. A3-11

$$SA_E = b(\emptyset_E - 1) + \ SA_{sphere} \,\#(A3 - 13)$$

Rearranging Eq. A3-13, the *b* constant can be described as

$$b = \frac{SA_{sphere} - SA_E}{1 - \emptyset_E} \#(A3-14)$$

Substituting Eq. A3-14 to Eq.A3-12, the *c* constant can be described as

$$c = SA_{sphere} - \frac{SA_{sphere} - SA_E}{1 - \emptyset_E} \#(A3-15)$$

Substituting Eq. A3-14 and Eq. A3-15 to Eq. A3-10, the surface area of the bolus can be described as

$$A_{Ob} = \frac{SA_{sphere} - SA_E}{1 - \emptyset_E} (\emptyset - 1) + SA_{sphere} \#(A3-16)$$

The initial surface area of the bolus, SA_E, can be estimated using equation A3-9. Thus,

$$SA_E = 4\pi (1+a)^{\frac{2}{3}} \sum_i^{n_p} r_i^2 \#(A3-17)$$

where

$$a = \frac{\varepsilon}{1-\varepsilon}.S \#(A3-18)$$

The total volume of particles can be described as below

$$V_{ptotal} = \frac{4}{3}\pi \sum_i^{n_p} r_i^3 \#(A3-19)$$

The total volume of the bolus is therefore

$$V_{bolus} = \frac{V_{ptotal}}{1 - \varepsilon} \#(A3-20)$$

If *R* is the radius of the bolus, the volume of the bolus can also be described as

$$V_{bolus} = \frac{4}{3}\pi R^3 \#(A3-21)$$

Equating Eq.A3-20 and Eq.A3-21, the radius of the bolus can be calculated as follows

$$R = \left(\frac{\sum_i^{n_p} r_i^3}{1-\varepsilon}\right)^{\frac{1}{3}} \#(A3-22)$$

Therefore, the surface area of the bolus when at 100% saturation (assuming spherical shape) is

$$SA_{sphere} = 4\,\pi\, R^{\frac{2}{3}} \#(A3-23)$$

Finally, the packing density of the bolus in Equation A3-16 can be estimated as described below

$$\emptyset = (1-\ \varepsilon) +\ S.\varepsilon \#(A3-24)$$

where the saturation of the bolus, S is calculated using the equation below

$$S = \frac{V_{opasted} + V_s}{V_{ptotal}} . \left(\frac{1-\varepsilon}{\varepsilon}\right) \#(A3-25)$$

Appendix A4 – Comparison between fitted D-values and pasted fraction which represents the PSD against experimental data for the remaining four subjects (A1, A2, A3, A5)

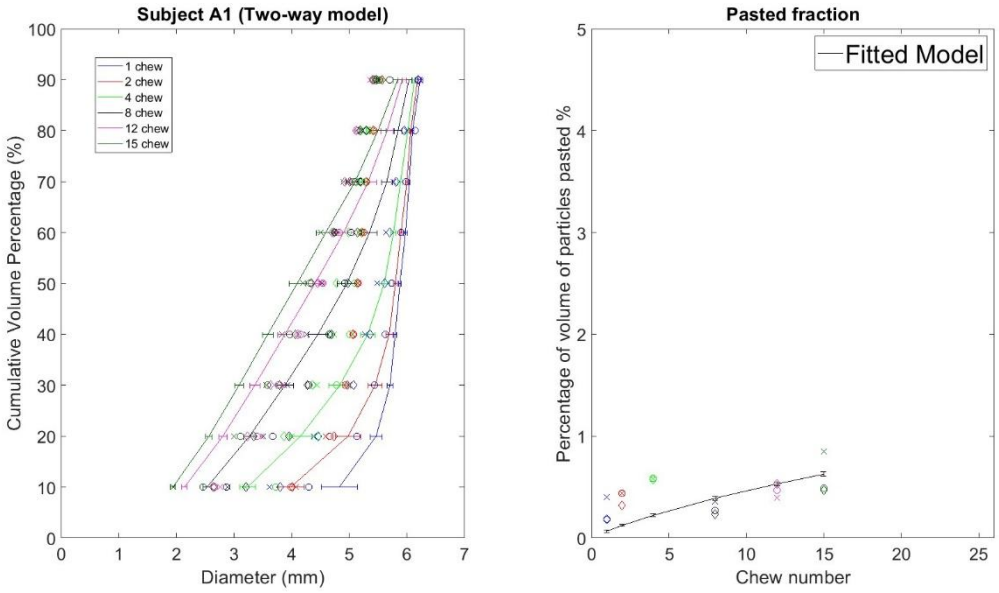

Figure A4-1. Best-fit model against experimental data for Subject A1. Two-way interaction model was used as the selection model. The plot on the left of the image is the comparison of the d-values of the best fit model and the experimental data whereas the plot on the right shows the comparison of the pasted fraction values. The error-bar of the model is the standard deviation of 50 simulations. All 3 replicates of the measured data (three different markers) were plotted for comparison.

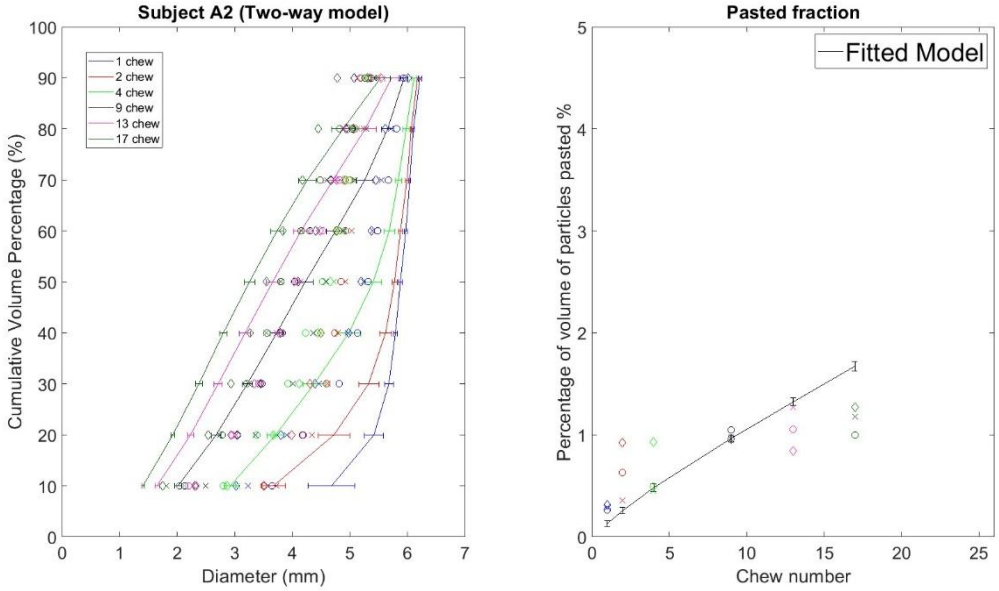

Figure A4-2.: Best-fit model against experimental data for Subject A2. Two-way interaction model was used as the selection model. The plot on the left of the image is the comparison of the d-values of the best fit model and the experimental data whereas the plot on the right shows the comparison of the pasted fraction values. The error-bar of the model is the standard deviation of 50 simulations. All 3 replicates of the measured data (three different markers) were plotted for comparison.

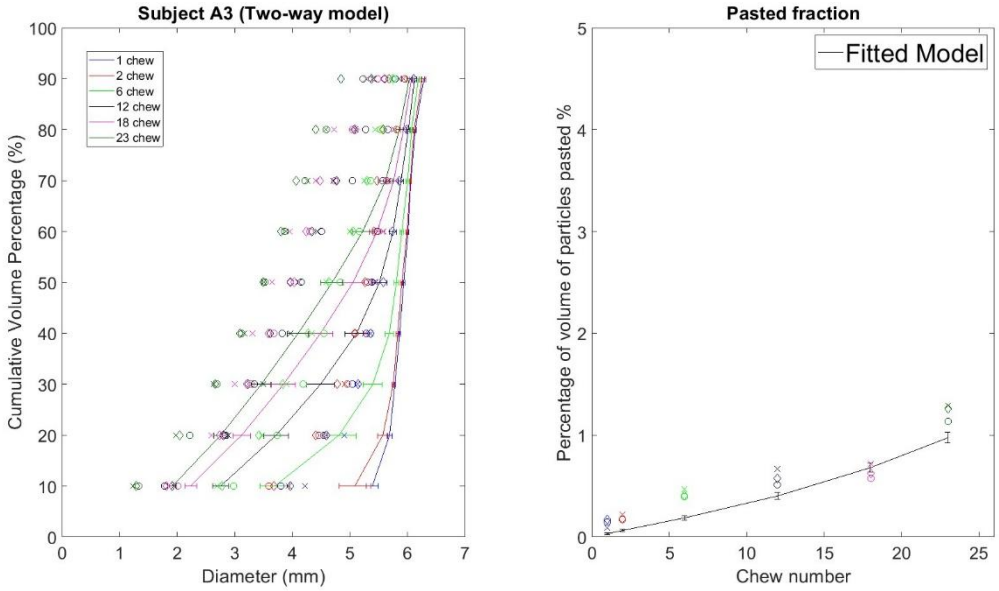

Figure A4-3. Best-fit model against experimental data for Subject A3. Two-way interaction model was used as the selection model. The plot on the left of the image is the comparison of the d-values of the best fit model and the experimental data whereas the plot on the right shows the comparison of the pasted fraction values. The error-bar of the model is the standard deviation of 50 simulations. All 3 replicates of the measured data (three different markers) were plotted for comparison.

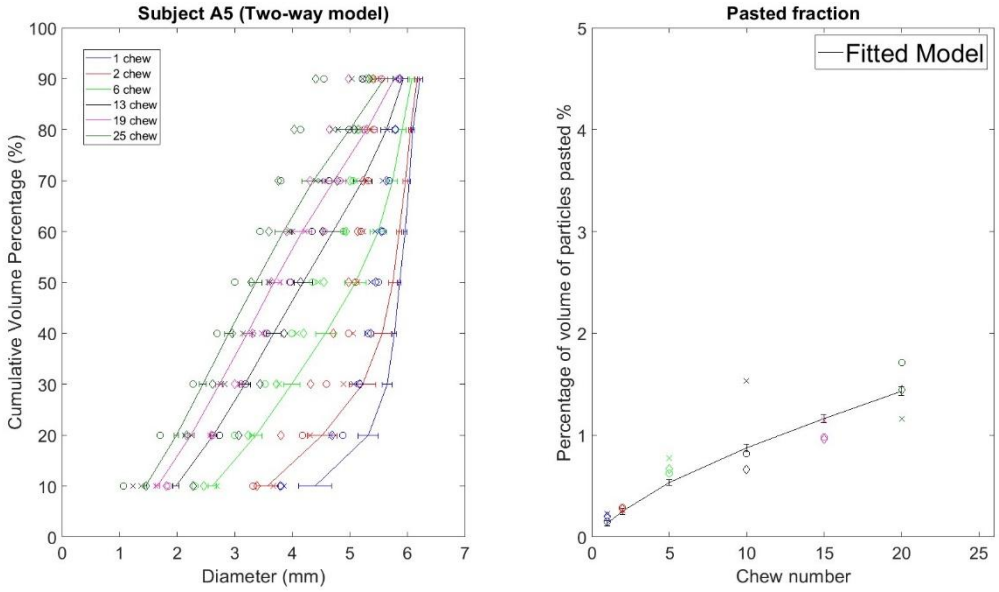

Figure A4-5. Best-fit model against experimental data for Subject A5. Two-way interaction model was used as the selection model. The plot on the left of the image is the comparison of the d-values of the best fit model and the experimental data whereas the plot on the right shows the comparison of the pasted fraction values. The error-bar of the model is the standard deviation of 50 simulations. All 3 replicates of the measured data (three different markers) were plotted for comparison.

Appendix A5 – Comparison between model predictions (coupled integrated selection –breakage and aroma release model) against experimental data for the remaining four subjects (A1, A2, A3, A5)

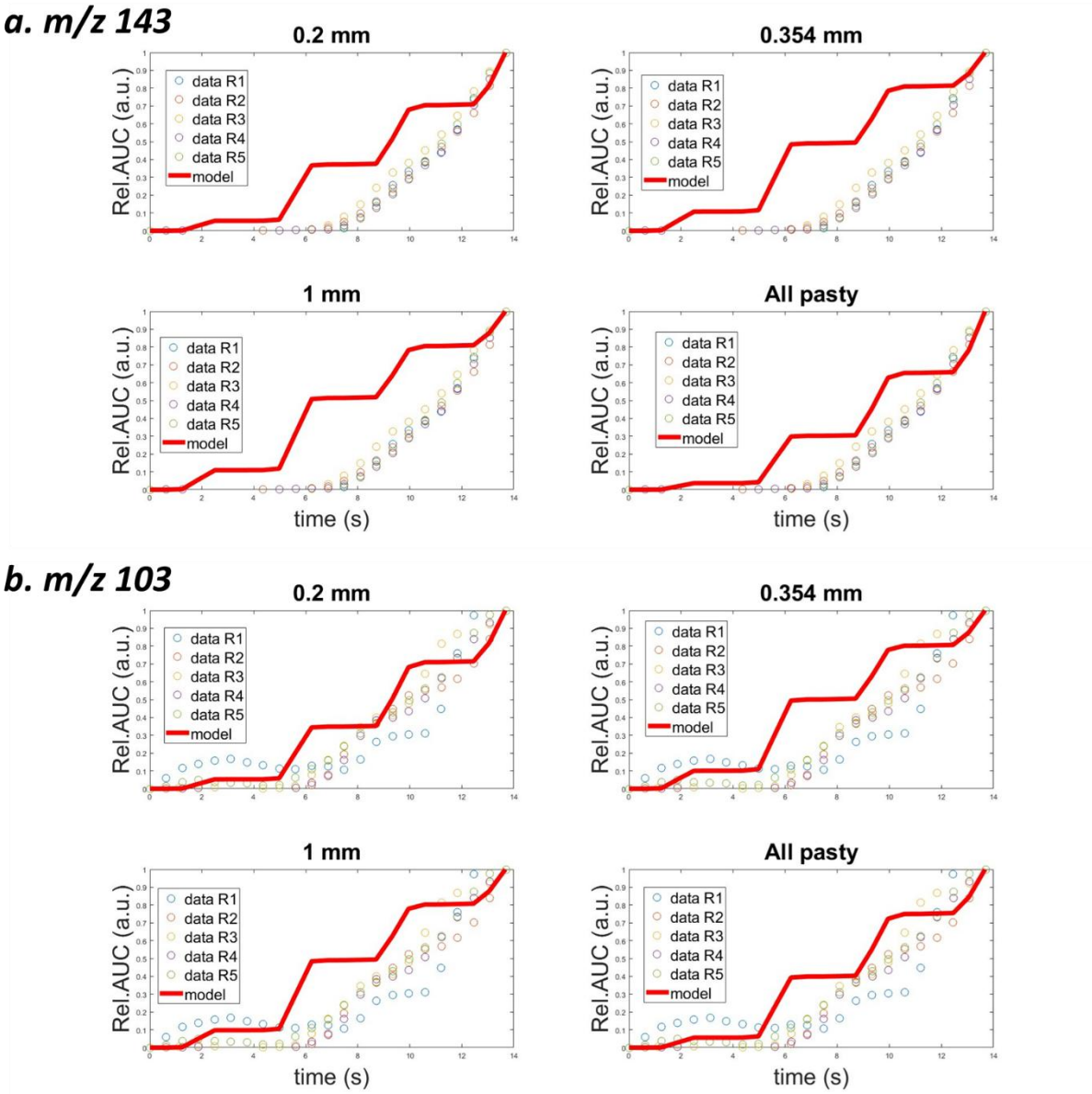

Figure A5-1. Model prediction against experimental data of 2-nonanone (m/z 143) and ethyl propanoate (m/z 103) for Subject A1. Rel. AUC refers to the relative cumulative area under the curve, where the cumulative area under the curve was normalised against the total area under the curve.The model was also predicted using different pasted size threshold (0.2 mm, 0.354 mm, 1 mm and when all particles were pasted) and compared against the five replicates of the experimental data.

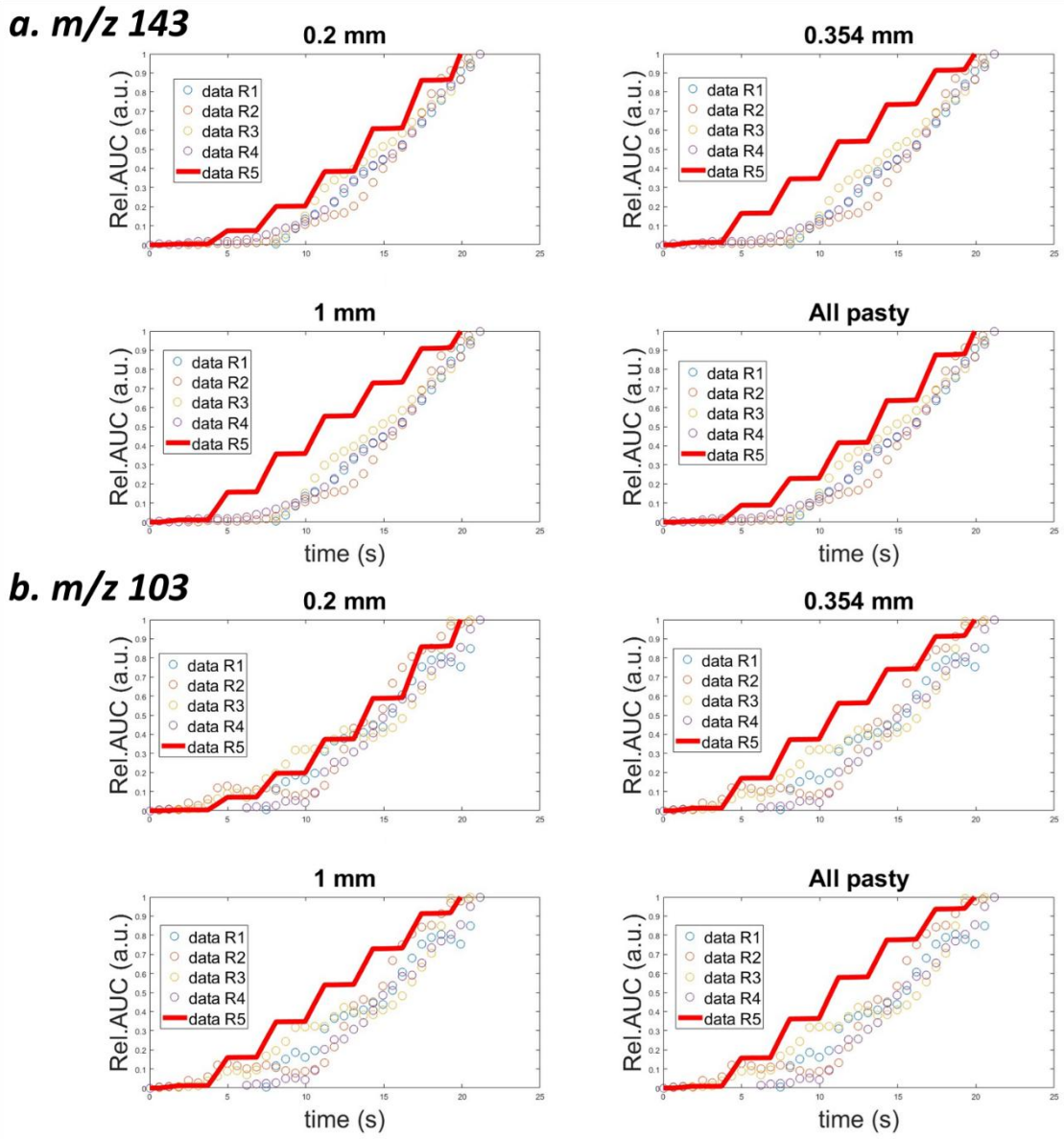

Figure A5-2. Model prediction against experimental data of 2-nonanone (m/z 143) and ethyl propanoate (m/z 103) for Subject A2. Rel. AUC refers to the relative cumulative area under the curve, where the cumulative area under the curve was normalised against the total area under the curve. The model was also predicted using different pasted size threshold (0.2 mm, 0.354 mm, 1 mm and when all particles were pasted) and compared against the five replicates of the experimental data.

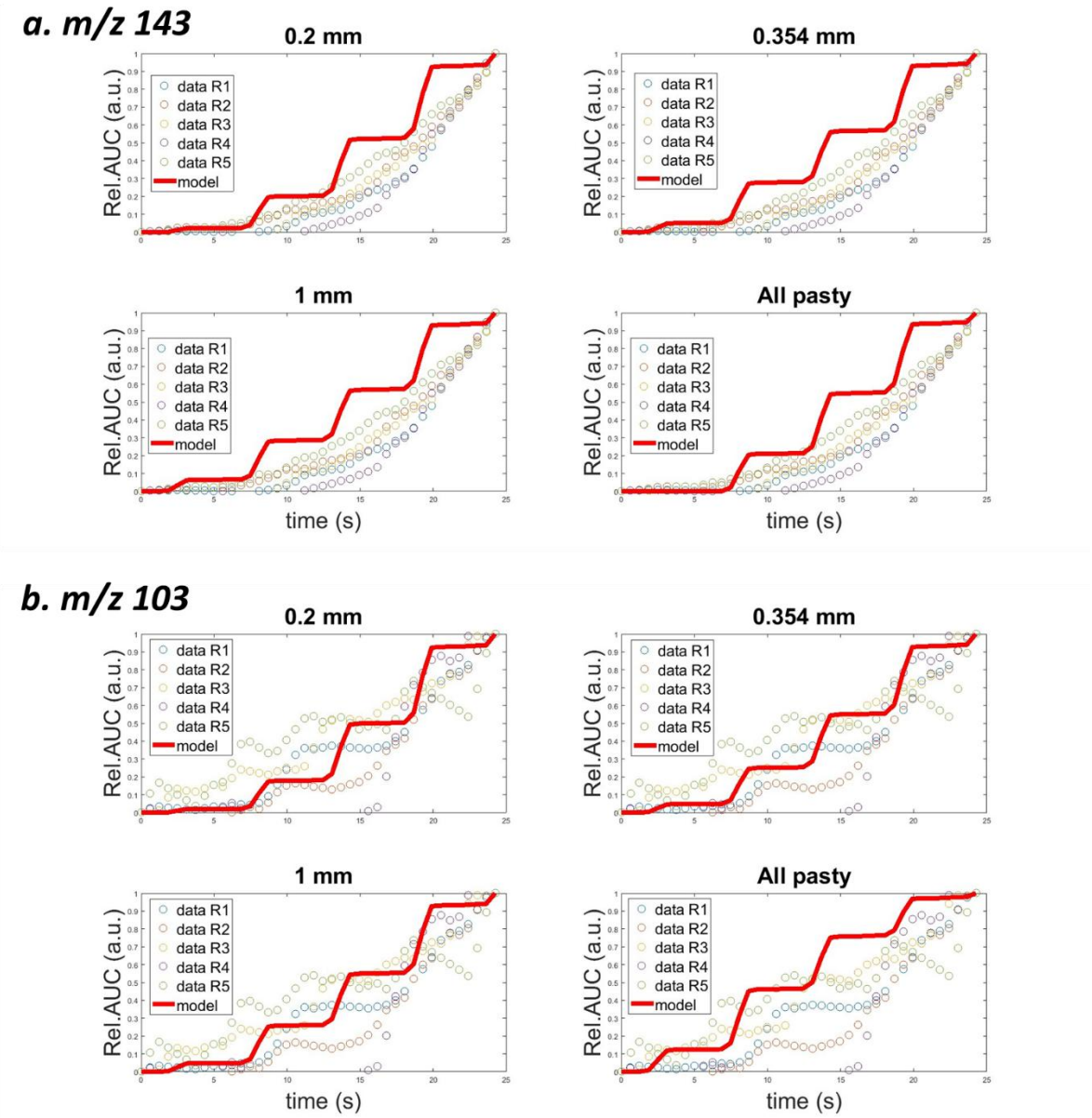

Figure A5-3. Model prediction against experimental data of 2-nonanone (m/z 143) and ethyl propanoate (m/z 103) for Subject A3. Rel. AUC refers to the relative cumulative area under the curve, where the cumulative area under the curve was normalised against the total area under the curve. The model was also predicted using different pasted size threshold (0.2 mm, 0.354 mm, 1 mm and when all particles were pasted) and compared against the five replicates of the experimental data.

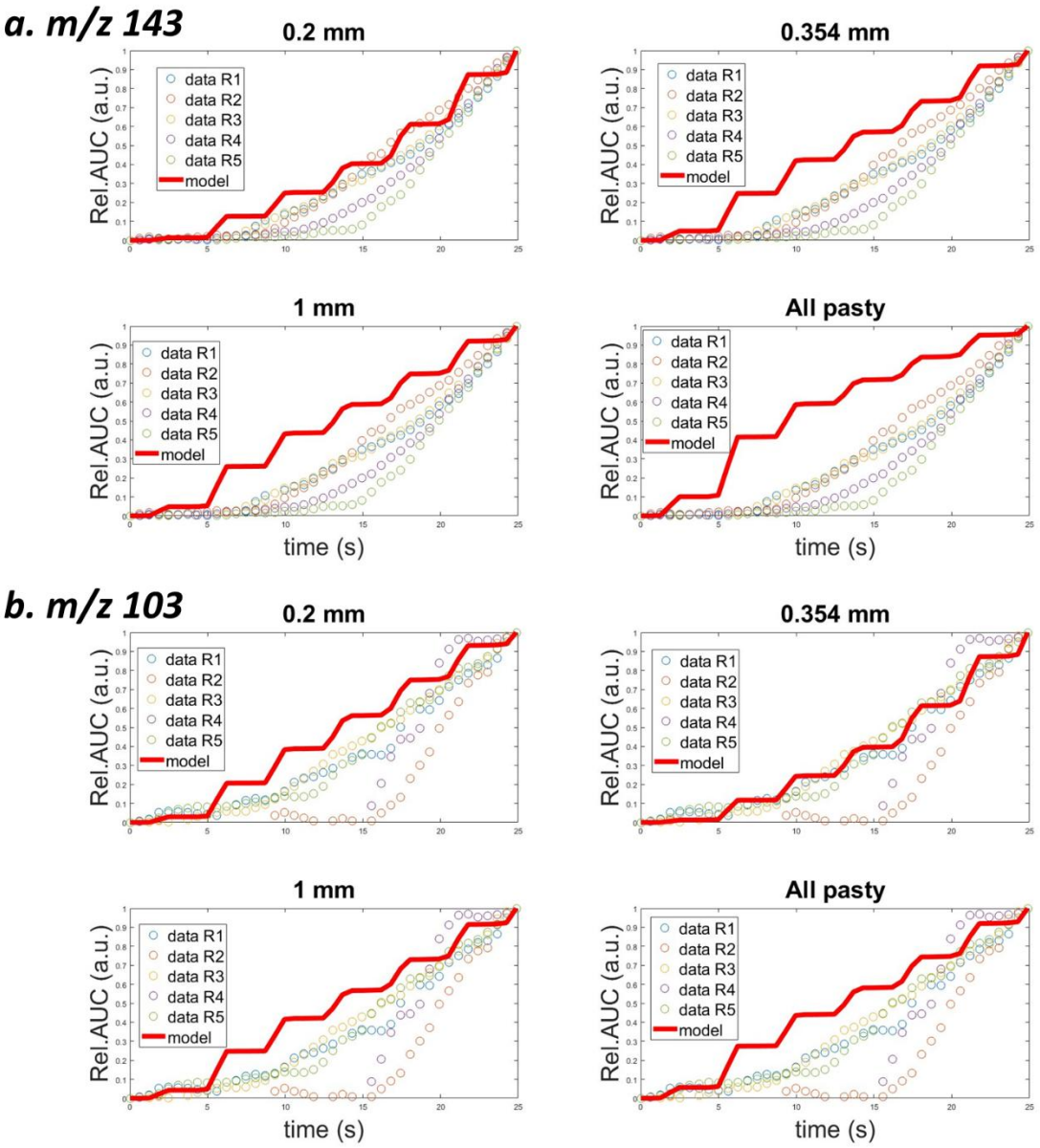

Figure A5-4. Model prediction against experimental data of 2-nonanone (m/z 143) and ethyl propanoate (m/z 103) for Subject A5. Rel. AUC refers to the relative cumulative area under the curve, where the cumulative area under the curve was normalised against the total area under the curve. The model was also predicted using different pasted size threshold (0.2 mm, 0.354 mm, 1 mm and when all particles were pasted) and compared against the five replicates of the experimental data.

Appendix A6– Subject's physiological input parameters

Table A6-1 defines the subject's physiological input parameters used in the model.

Table A6-1 Subject's physiological input values used in the model

Symbol	Unit	Description	Reference value	Range of variation	Source
A_O	m^2	Total area in oral cavity	1.2×10^{-2}	1.2×10^{-3}- 2.3×10^{-2}	(Déléris et al., 2016; Doyennette et al., 2014)
A_F	m^2	Total area of the pharynx	6.5×10^{-3}	3.3×10^{-3}- 1.3×10^{-2}	(Déléris et al., 2016; Doyennette et al., 2014)
A_{Oam}	m^2	air/lubricated mucosa contact area in the oral cavity	$= 10^{-1} \times A_O$	$10^{-1} \times A_O$ - A_O	(Déléris et al., 2016)
A_{Fam}	m^2	air/lubricated mucosa in the pharynx	$= 10^{-1} \times A_F$	$= 10^{-1} \times A_F$ – A_F	(Déléris et al., 2016)
A_{Fas}	m^2	air/saliva contact area in the pharynx	$= A_F$ - A_{Fam}	/	(Déléris et al., 2016)
A_{Nam}	m^2	air/lubricated mucosa in the nasal cavity	1.5×10^{-2}	7.5×10^{-4} - 3×10^{-2}	(Déléris et al., 2016)
e_{Oam}	m	Thickness of wetted mucosa in the oral cavity	5×10^{-5}	5×10^{-6}- 5×10^{-4}	(Déléris et al., 2016)
e_{Fam}	m	Thickness of wetted mucosa in the pharynx	5×10^{-5}	5×10^{-6}- 5×10^{-4}	(Déléris et al., 2016)
e_{Nam}	mm	Thickness of mucosa in nasal cavity	5×10^{-5}	5×10^{-6}- 5×10^{-4}	(Déléris et al., 2016)
F_{breath}	number of cycles/s	breathing frequency	0.26	0.25-0.33	Experimental values
fr_{chew}	number of chews/s	chewing frequency	1.3	1.2-1.4	Experimental values
$fr_{opening}$	occurrence number/s	opening frequency of the velopharynx	= F_{breath} or fr_{chew}	/	(Doyennette et al., 2014)
V_c	m^3	current breath volume	8×10^{-4}	8×10^{-4} -1.6 $\times 10^{-3}$	(Déléris et al., 2016; Doyennette et al., 2014)
V_{Osrest}	m^3	volume of saliva at rest in the oral cavity	3.6×10^{-7}	1×10^{-7}-1 8.7×10^{-7}	Experimental values

V_{Om}	m^3	volume of mucosa in the oral cavity	= $e_{Oam} x A_{Oam}$	/	(Déléris et al., 2016)
V_{Oamean}	m^3	volume of air in the oral cavity	6.4×10^{-5}	5.7×10^{-5}- 6.8×10^{-5}	Experimental values
V_{Fa}	m^3	volume of air in the pharynx	3.4×10^{-5}	2.9×10^{-5}- 4.2×10^{-5}	Experimental values
V_{Fs}	m^3	volume of saliva in the pharynx	2×10^{-7}	2×10^{-7} – 4×10^{-7}	(Déléris et al., 2016)
V_{Fm}	m^3	volume of mucosa in the pharynx	= $e_{Fam} x A_{Fam}$	/	(Déléris et al., 2016)
V_{Na}	m^3	volume of air in the nasal cavity	1.45×10^{-5}	1.03×10^{-5}- 1.95×10^{-5}	Experimental values
V_{Nm}	m^3	volume of mucosa in the nasal cavity	= $e_{Nam} x A_{Nam}$	/	(Déléris et al., 2016)
Q_{Os}	m^3/s	saliva flow rate in the oral cavity	4×10^{-8}	1.8×10^{-8}- 1.8×10^{-8}	Experimental values
$t_{swallow}$	s	time taken to swallow	20	12-20	Experimental values
n_{chews}		number of chews required to reach swallow point	28	15-38	Experimental values

Appendix A7– Physico-chemical parameters

Table A7-1 defines the physico-chemical parameters used in the model.

Table A7-1: Physico-chemical parameters used in the model.

Symbol	Unit	Description	Reference value	Range of variation	Source
k_{Os}	m/s	mass transfer coefficient in the saliva phase in the oral cavity	10^{-6}	10^{-8}-10^{-4}	(Déléris et al., 2016)
k_{Fs}	m/s	mass transfer coefficient in the saliva phase in the pharynx	10^{-6}	10^{-8}-10^{-4}	(Déléris et al., 2016)
k_{Om}	m/s	mass transfer coefficient in the lubricated mucosa in the oral cavity	10^{-6}	10^{-8}-10^{-4}	(Déléris et al., 2016)
k_{Fm}	m/s	mass transfer coefficient in the lubricated mucosa in the pharynx	10^{-6}	10^{-8}-10^{-4}	(Déléris et al., 2016)
k_{Nm}	m/s	mass transfer coefficient in the lubricated mucosa in the nasal cavity	10^{-6}	10^{-8}-10^{-4}	(Déléris et al., 2016)
K_{Oas}		air/saliva partition coefficient in the oral cavity **at 37°C**	12.9×10^{-3} (**Ethyl propanoate**) 9.7×10^{-3} (**2-nonanone**)	/	(Déléris et al., 2016)
K_{Osp}		saliva/product(rice) partition coefficient in the oral cavity **at 37°C**	2.14 (**Ethyl propanoate**) 2.5×10^{-1} (**2-nonanone**)	/	Experimental values
K_{Oam}		air/lubricated mucosa partition coefficient in the oral cavity	10^{-3}	10^{-5}-10^{-1}	(Déléris et al., 2016)
K_{Fas}		air/saliva partition coefficient in the pharynx	5×10^{-3}	5×10^{-4}- 5×10^{-2}	(Déléris et al., 2016)
K_{Fam}		air/lubricated mucosa partition coefficient in the pharynx	10^{-3}	10^{-5}-10^{-1}	(Déléris et al., 2016)
K_{Nam}		air/lubricated mucosa partition coefficient in the	10^{-3}	10^{-5}-10^{-1}	(Déléris et al., 2016)

C_{Op}	kg/m^3	nasal cavity aroma concentration in the product (rice) in the oral cavity	1.5 x 10^{-4} (ethyl propanoate) 4.8 x 10^{-3} (2-nonanone)	/	Experimental values